# Physiologic Targets and Modes of Action for CBL0137, a Lead for Human African Trypanosomiasis Drug Development

Carlos E. Sanz-Rodríguez[2], Benjamin Hoffman[2], Paul J. Guyett[2], Andrei Purmal[3], Baljinder Singh[4], Michael Pollastri[4], and Kojo Mensa-Wilmot[1,2]*

[1]Department of Molecular and Cellular Biology, Kennesaw State University, Kennesaw, GA
[2]Department of Cellular Biology, University of Georgia, Athens, GA
[3]Buffalo Biolabs INC, Buffalo, NY
[4]Department of Chemistry and Chemical Biology, Northeastern University, Boston, MA

**RUNNING PAGE TITLE**

*Running Page Title*: Polypharmacology of CBL0137 in the African Trypanosome

Correspondence: kmensawi@kennesaw.edu

Kojo Mensa-Wilmot

Department of Molecular and Cellular Biology,

Kennesaw State University, Kennesaw, GA 30144

Total number of manuscript pages, 42

Figures, 10

Tables, 1.

Total word count of the Abstract (221)

Introduction (668)

Discussion (1060)

Non-standard abbreviations: DCC, delayed cytocidal concentration

## ABSTRACT

CBL0137 is a lead drug for human African trypanosomiasis, caused by *Trypanosoma brucei*. Herein, we use a four-step strategy to (a) identify physiologic targets and (b) determine modes of molecular action of CBL0137 in the trypanosome. First, we identified fourteen CBL0137-binding proteins using affinity chromatography. Second, we developed hypotheses of molecular modes of action, using predicted functions of CBL0137-binding proteins as guides. Third, we documented effects of CBL0137 on molecular pathways in the trypanosome. Fourth, we identified physiologic targets of the drug, by knocking down genes encoding CBL0137-binding proteins and comparing their molecular effects to those obtained when trypanosomes were treated with CBL0137. CBL0137-binding proteins included glycolysis enzymes (aldolase, glyceraldehyde-3-phosphate dehydrogenase, phosphofructokinase, phosphoglycerate kinase), and DNA-binding proteins (UMSBP2, RPA1, RPA2). In chemical biology studies CBL0137 did not reduce ATP level in the trypanosome, ruling out glycolysis enzymes as crucial targets for the drug. Thus, many CBL0137-binding proteins are not physiologic targets of the drug. CBL0137 inhibited (i) nucleus mitosis, (ii) nuclear DNA replication, and (iii) polypeptide synthesis as the first carbazole inhibitor of eukaryote translation. RNAi against RPA1 inhibited both DNA synthesis and mitosis, whereas RPA2 knockdown inhibited mitosis, consistent with both proteins being physiologic targets of CBL0137. Principles used here to distinguish drug-binding proteins from physiologic targets of CBL0137 can be deployed with different drugs in other biological systems.

**SIGNIFICANCE STATEMENT**

To distinguish drug-binding proteins from physiologic targets in the African trypanosome we devised and executed a multi-disciplinary approach involving biochemical, genetic, cell, and chemical biology experiments. The strategy we employed can be used for drugs in other biological systems.

## INTRODUCTION

Human African trypanosomiasis (HAT) is caused by *Trypanosoma brucei gambiense* and *T.b. rhodesiense*. Being a zoonotic disease transmitted by tsetse flies, a reservoir of *T. brucei* in non-human vertebrates in the wild is a significant problem for elimination. HAT is managed with chemotherapy: Fexinidazole, the first new drug in fifty years was approved in 2018 for treatment of HAT caused by *T. b. gambiense* (Lindner et al., 2020; Pollastri, 2018; Watson et al., 2019). Limitations of current medications call for continued work to discover new drugs. In the case of fexinidazole, patients' non-compliance is an issue because of nausea and vomiting. Further, recrudescence of HAT is reported after treatment (Sokolova et al., 2010) (Pelfrene et al., 2019). Thus, there is need to find new drugs against HAT, but only one drug, acoziborole (SCYX-7158) is currently in clinical trials (Jacobs et al., 2011; Jones et al., 2015).

Phenotypic (*i.e.*, whole cell) screening has made important contributions to discovery of hits for infectious diseases (Butera, 2013; Ferguson et al., 2019; Patra et al., 2020; Swinney and Anthony, 2011). In anti-parasite drug development, there is significant evidence for prominence of "phenotypic screening" in drug discovery (Buckner et al., 2020): SCYX-7158 entered Phase II clinical trials for HAT without knowledge of its target (Thomas et al., 2016a), and only recently have "modes of action" (MOA) studies received attention (Kaiser et al., 2011; Koman et al., 2012; Torreele et al., 2010). Phenotypic screening is also important for discovering hits against some cancers, neurological and chronic diseases (Abo-Rady et al., 2019; Bryce et al., 2019; Drowley et al., 2020; Keatinge et al., 2021; Ruillier et al., 2020; Shapovalov et al., 2021; Swalley, 2020; Wang et al., 2020; Weng et al., 2019).

Curaxins are carbazole derivatives with acyl substituents at positions 3- and 6- of the scaffold, and a pendant secondary or tertiary amino group that is separated by 2-to-4 carbon atoms from the carbazole nitrogen. Curaxin CBL0137 is undergoing phase I clinical evaluation and is active against some human cancer cell lines. CBL0137 has several modes of action, including chromatin remodeling, in mammalian cells (Koman et al., 2012; Sergeev et al., 2020).

In anti-trypanosome drug development, CBL0137 emerged as a lead drug from phenotypic screening (Thomas et al., 2016b). Consequently, neither its target nor mechanism of action is known. In this study we have attempted to find CBL0137-binding proteins in trypanosomes, using drug affinity chromatography. Fourteen CBL0137-binding proteins were discovered, and they were used to develop hypotheses regarding possible modes of anti-trypanosome action of CBL0137. Next, we screened the CBL0137-binding proteins for as possible physiologic targets of the drug since binding of the drug to many proteins may have no biologically significant effects *in vivo*. For example, plasma proteins bind drugs but are not considered physiological targets of the small molecules. A "physiological target of a drug" may be defined as a gene whose knockdown (or over-expression) yields very similar/identical molecular effects as treatment of cells with the drug. Genes encoding CBL0137-binding proteins were knocked down, and the molecular effects compared to those obtained from perturbation of trypanosomes with the drug. The expectation was that when a physiological target was knocked down the molecular defects reported would be very similar to those obtained when the drug was added to trypanosomes. The principle of expecting a drug to "phenocopy" knockdown of its physiological target has been established by the Shapiro (Meyer and Shapiro, 2021) and Mensa-Wilmot laboratories (Guyett et al., 2016).

Our systematic and multi-disciplinary strategy revealed concentration-dependent selectivity in modes of action for the drug. CBL0137 inhibited both nuclear DNA replication and nucleus segregation (*i.e.,* mitosis) at low concentrations (less than 180 nM). At higher concentration (*i.e.,* above 280 nM) the drug blocked protein synthesis. Of fourteen CBL0137-binding proteins documented, data obtained for RPA1 and RPA2 are consistent them as physiologic targets of CBL0137. We concluded that CBL0137 is a multi-target drug that affects three biological pathways (DNA replication, synthesis of proteins, and nucleus segregation) in the African trypanosome.

## Methods

*Cell and culture conditions.* Bloodstream *T. brucei* Lister 427, single marker (SM) (Wirtz et al., 1999), and specific trypanosome lines for RNAi (RPA1-RNAi, RPA2-RNAi, UMSBP2-RNAi, eIF4A1-RNAi (Supplementary Material), were cultured in HMI-9 medium (Hirumi and Hirumi, 1989) supplemented with 10% tetracycline-free fetal bovine serum (Atlanta Biologicals, Flowery Branch, GA), and 10% Serum Plus (Sigma-Aldrich) at 37˚C, 5% $CO_2$. (Primers used for preparation of RNAi constructs are described in Supp. Table S2.) Antibiotics for parasite maintenance of stable trypanosome lines were hygromycin (5 µg/ml), G418 (6.4 µg/ml), puromycin (0.5 µg/ml) and blasticidin (5 µg/ml).

*Delayed Cidality Assays.* Parasites ($10^3$ cells/ml or $10^5$ cells/ml) were incubated with different concentrations of CBL0137 or DMSO (0.1%) for 6h. Then, cells were washed, resuspended in fresh medium at $10^4$ trypanosomes per ml, and incubated for 48 h. Trypanosomes were enumerated with a Coulter-Counter (Beckman).

5-Ethynyl-2'-deoxyuridine *(EdU) assays.* Bloodstream trypanosomes (5 x$10^5$ cells/ml) were preincubated for 15 min with different concentrations of the drugs (in HMI-9 medium), 5-ethynyl-2'-deoxyuridine (EdU) (Abcam) was added to 300 µM (final concentration) and cells were incubated for 1 h. Cells were prepared as previously described (Sullenberger et al., 2017). Images of trypanosomes were captured using a DeltaVision II Olympus inverted microscope (Fig. 2) or Keyence BZ-X800 (Fig. 9), and data was processed with Fiji (ImageJ, v 2.0.0). Images were masked in the nuclei area, and the pixel intensity for each image was stretched until getting the entire intensity range. Finally, all pixel values were added (integrated), and the resulting value, named integrated intensity, was plotted. Data for integrated intensity was processed using CellProfiler 3.1.9 (McQuin et al., 2018).

*Protein synthesis assay.* Trypanosomes were cultured to late log-phase (between $2 \times 10^5$/ml and $1 \times 10^6$/ml). Cells were harvested, washed, and resuspended ($5 \times 10^5$ cells/ml) in RPMI without methionine supplemented with 10% fetal bovine serum, and incubated for 15 min with different concentrations of drugs. L-Homopropargylglycine (HPG, Cayman chemical) was added (to 4 μM), followed by incubation for 1 h at room temperature. Cells were harvested, washed with PBS-G (PBS with 10 mM glucose), pelleted ($\sim 5 \times 10^6$ cells), and resuspended in 50 μl of permeabilization buffer (50 mM HEPES pH 7.4, 0.025% NP-40) on ice for 30 min. Fifty μl of "click-chemistry" cocktail (20 mM Tris buffer, pH 7.4, 5 mM CuSO4, 300 mM ascorbic acid , 140 mM NaCl, and 17.5 μM azide-PEG-biotin) was added, and the mixture was incubated at room temperature for 1 h. Proteins were precipitated by adding 400 μl of ice-cold acetone, pelleted (4 °C, 20 min, 20,000 x $g$), dried, and resuspended in SDS sample buffer ($1 \times 10^5$ cells/μl). Proteins were heated at 95 °C for 5 min, and separated by SDS-PAGE (12%), transferred onto low fluorescence PVDF membrane (Bio-Rad), and developed with streptavidin-IRDye 800CW (Li-COR) (1:2500 dilution). Images were captured with an Odyssey® CLx imaging system (Li-Cor), and data were processed using Empiria Studio® Software (Li-Cor).

*Preparation of Curaxin-agarose drug affinity column:* The preparation of the alkyne derivative of CBL0137 (Table 1 Image) is reported in the Supporting Information (Supp. Scheme 1 and Supp. Scheme 2). This compound was coupled to azide agarose-beads using copper-catalyzed click-chemistry (Punna et al., 2005; Rostovtsev et al., 2002), following recommendations in a tris-hydroxypropyltriazolylmethylamine (THPTA)-based click kit (Jena Biosciences). Agarose-azide beads (125 μl settled bed volume) (Jena Bioscience CLK-1038-2) were mixed with 0.5% DMSO (negative control) or alkyne derivative of CBL0137 (10 mM) in presence of CuSO$_4$ (2 mM), THPTA (10 mM), sodium ascorbate [100 mM in sodium phosphate (NaPi) buffer, pH 7.2]. The

beads were vortexed and then incubated on a rotary mixer for 2 h at room temperature, washed twice with 200 µl PBS for 20 min before use.

*Affinity chromatography with Curaxin Class 3-agarose:* T. brucei Lister 427 were axenically cultured in HMI-9 medium to a density of $10^6$ cells/ml, harvested, and washed in cold PBS-G. Cells ($10^8$) were resuspended in 1 ml of lysis buffer (50 mM sodium phosphate, pH 7.2; 100 mM NaCl, 0.1% NP-40, 5% glycerol, and HALT protease inhibitor cocktail (Thermofisher)). Trypanosomes were sonicated in an ice bath with a QSonica, LCC sonicator, model Q55 at amplitude set to 45, 3 cycles of "30 seconds on and 2 min off". Sonicated mixture was diluted two-fold with cold PBS, and 100 µl of pre-cleared (12,000 x g, 5 min, 4°C) lysate ($10^8$ trypanosome equivalent) was applied to Curaxin-agarose (100 µL) or to an equivalent volume of agarose beads (negative control). The lysate was incubated with the beads at 4°C overnight and washed with 500 µL of cold PBS five times. Bound proteins were eluted by incubating beads with 200 µL PBS containing CBL0137 (50 µM) for 1 h, 4°C. Eluted proteins were resolved by SDS-PAGE (12%) and stained with Pierce™ Silver for Mass Spectrometry kit (Pierce) to visualize polypeptide bands.

*Mass spectrometry analysis:* Proteins from Curaxin-affinity column or agarose beads were extracted from the gel and prepared for mass spectrometry as described previously (Guyett et al., 2016). Tryptic peptides were purified using the C18 column (ZipTip) (Millipore Corporation) and divided into two technical replicates for LC-MS/MS analysis on an Easy-nLC 1000 (Thermo Scientific) coupled to an Orbitrap Fusion mass spectrometer (Thermo Scientific). LC and MS run conditions were used as previously described (Guyett et al., 2016). The mass spectrometer was operated in a data-dependent MS/MS mode. The most abundant ions from the precursor scan were selected for MS/MS analysis using high-energy collisional dissociation (HCD) and analyzed with an ion trap. Data from technical replicates were combined, analyzed using

Proteome Discoverer 2.0 (ThermoScientific), and searched with SEAQUEST (Eng et al., 1994) against a *T. brucei* database (tritrypdb.org) that included common contaminants. Trypsin was set as the protease with maximum missed cleavages fixed at two. The precursor ion tolerance was set to 10 ppm, and the fragment ion tolerance was set to 0.6 Da. Variable modifications were methionine oxidation (15.995 Da) and phosphorylation (79.966) on serine, threonine, and tyrosine. Search results were run through Percolator (Kall et al., 2007) for scoring. Results were filtered for peptides with a false-discovery rate (FDR) of 0.05. The number of peptide spectrum matches (spectral counts) for each protein were obtained in three independent experiments. PEP-values for each peptide were calculated in Proteome Discoverer 2.0 (ThermoScientific).

*Antibodies*: Antibodies (named) were used at the following dilutions: YL1/2 (EMD Millipore; Billerica, MA) against TbRP2 (Andre et al., 2014) at 1:2500; rabbit anti-V5 (D3H8Q) (Cell Signaling; Danvers, MA) at 1:1000 for immunofluorescence and 1:3000 for western blotting. Anti-Myc mouse monoclonal (9E10) (Santa Cruz), 1:2000 for western blots. Secondary antibodies for immunofluorescence were conjugated to either Alexa Fluor-488 (AF-488) or AF-594 (Invitrogen) and were used at 1:3000 dilution. Anti-mouse or anti-rabbit IRDye secondary antibodies 800CW (Li-Cor, Lincoln, NE) were used for western blots at 1:20000 dilution. Epitope-tagging of trypanosomes (Shen, 2001) was performed with primers presented in supplemental methods (Supp. Table S3).

*Immunofluorescence*. Trypanosomes were pelleted by centrifugation, rinsed once with PBS-G, fixed with paraformaldehyde (4% in PBS) for 20 min, and applied to a coverslip pre-coated with poly-L-lysine. The coverslip was rinsed in PBS, and then in 100 mM $NH_4Cl$/100mM glycine for 10 min to quench the fixation of cells. Trypanosomes were rinsed thrice with PBS, 5 min each time, and incubated for 1h with a "Blocking and permeabilizing solution" [PBS, fish-gelatin (1X; Biotium), 1% BSA, 0.1% Tween-20]. Primary antibody was added for an hour, after which the

coverslip was rinsed thrice with PBS (as described earlier). Secondary antibody was then incubated with the coverslips in the blocking for 1h, rinsed three times with PBS, and then mounted on slides in Vectashield containing DAPI (5 µM) for image acquisition.

*Western blotting.* Trypanosomes were collected by centrifugation and washed with PBS-G. Cells were lysate by direct resuspension in SDS-sample buffer + 1 mM of β-mercaptoethanol with final density of $1 \times 10^5$ or $3 \times 10^5$ of cells/µl and boiled for 5 min at 95 ˚C. 10 µl of sample was loaded in each lane ($1-3 \times 10^6$ cell equivalents per sample). Proteins were separated on TGX Fast-Cast™ acrylamide (12%) gel (Bio-Rad, Hercules, CA), and transferred to LF-PVDF membrane using a Trans-Blot Turbo system (Bio-Rad). The membrane was treated with Revert™ total protein stain for WB (LI COR, Lincoln, NE) in PBS-based Intercept (Intercept-PBS) blocking solution. Primary antibody was added in Intercept-PBS/0.2% of Tween-20. Secondary antibody was used in Intercept-PBS/ 0.2% Tween-20/0.01% of SDS. Empiria Studio Software (LI COR) was used to measure the intensity of the secondary antibody signal (at 800 nm) for each antigen. For each lane, normalization was carried out in Empiria Studio Software using a density integrity over the entire lane for each condition obtained at 700 nm (for Revert total protein stain). Western blots were performed in triplicate, and the normalized bands in each sample lane were averaged.

*Quantitation of total protein in western blots.* Cultures of a clonal line of *T. brucei* stably transfected with V5-NRP1 ($1 \times 10^5$ cells/ml) were incubated with or without DMSO, or CBL0137 (730 nM) for 6 h in HMI-9 medium, lysed and separated ($1 \times 10^6$ trypanosome equivalents per lane) in a TGX Fast-Cast™ Stain-free acrylamide (12%) gel (see section directly above). Images were acquired with a ChemiDoc XRS+ (Bio-Rad). The experiment was performed thrice with different biological samples. Values for total fluorescence in each lane was obtained using Fiji (ImageJ, v 2.0.0). To determine possible statistical significance of differences in total

fluorescence per lane a paired two-sided t-test (in Graphpad Prism 9.0) was used. (A representative image for gel from one experiment is presented Fig. 7B (lower panel, center)).

*Statistical Analysis*. For non-categorical data with few points, we implemented a two-side paired Student's t-test, or paired one-way ANOVA. A two-side Kolmogorov-Smirnov test was employed for data with a wide range and whose distribution was not normal, to test for significance of differences in the distribution. When distribution of distinct types of trypanosomes (categorical data) was analyzed, a Chi-squared ($x^2$) test was used to test for differences in distributions between different groups. All analyses were executed with GraphPad Prism 9.0. For all analysis $\alpha = 0.05$.

## RESULTS

**Determination of pharmacodynamically equivalent concentrations of drugs**

Major goals of our work were to (i) determine mechanisms of action of CBL0137 against trypanosome, and (ii) identify proteins that interacted with the drug. Since we planned to study control compounds, it was important to decide the concentration of each drug for each experiment. Here, we avoided using identical concentrations of drugs (per experiment) since their varying physicochemical properties result in non-equivalent quantities accumulating in trypanosomes. Given these considerations, we used an empirically determined drug concentration termed "delayed cidal concentration" (DCC) whose "readout" was relative trypanocidality. DCC assays (described below) are performed by treating cells for a short period with drugs, and washing drug off. The trypanosomes are viable immediately after treatment with drug (monitored by permeability to propidium iodide): Cidality is determined after culturing drug-treated cells for 48 h.

Experimentally, we determined DCC by treating trypanosomes ($10^5$/ml in culture medium) with varying concentrations of a drug for 6 h (Fig. 1). After washing the drug off, cells were resuspended in a fresh medium, cultured for 48 h, and trypanosome density quantitated. The concentration of drug that caused twenty-five, fifty, or ninety percent cidality, in comparison to DMSO-treated control trypanosomes, was termed $DCC_{25}$, $DCC_{50}$, and $DCC_{90}$, respectively (Fig. 1 and Supp. Table S1). $DCC_{25}$, for example, permits us to study early molecular effects of a drug on trypanosomes before cidal effects manifest.

For different drugs, $DCC_{25}$ determined with a fixed inoculum of cells (*e.g.*, 5 x $10^5$/ml) varied dramatically. For example, for CBL0137 and cycloheximide (CHX), $DCC_{25}$ values were 180 nM and 2840 nM, respectively (Supp. Table S1). These data are consistent with our suspicion that differences in drug properties affect concentrations needed for equivalent trypanocidality. Thus, DCC's represent pharmacodynamically equivalent amounts of drug. To determine modes of action of hits we used $DCC_{25}$ amounts for each drug in our studies.

In a parallel set of experiments, we determined drug concentrations required to limit proliferation (instead of cidality) of trypanosomes ($1 \times 10^5$/ml) in 6 h (*i.e.*, $GI_{25}$). For CBL0137 growth inhibitory (GI) concentration for 25, 50 and 90% (i.e., $GI_{25}$, $GI_{50}$ and $GI_{90}$) were 290 nM, 590 nM and 2540 nM respectively. Thus, in each case GI concentration was higher than the corresponding DCC. These data suggest that it is preferable to use DCC amounts of drug to study biological effects of curaxins because they are consistently lower than GI concentrations. Biological effects of drugs are best studied with the smallest nontoxic concentrations that can be used.

**Identification of CBL0137-binding Proteins, and Prediction of Biological Effects of CBL0137 on Bloodstream *T. brucei***

Drug-binding proteins can provide clues about the modes of action of small molecules. For that reason, we searched for trypanosome proteins that associate with CBL0137 using affinity chromatography. In our protocol, proteins from a trypanosome lysate were retained by a drug-agarose column (Fig. 2). Following several washes with PBS buffer, proteins were eluted with buffer containing CBL0137 (50 $\mu$M) and they were identified by liquid chromatography-mass spectrometry (Table 1). As a control, the trypanosome lysate was loaded on a column of azide-agarose, from which bound proteins were eluted with CBL0137 (Table 1). The experiment was performed thrice.  Data were filtered for peptides with a false-discovery rate (FDR) of 0.05, and the number of spectral counts for each protein were determined in the three independent experiments.

Four enzymes in the glycolysis pathway (fructose-bisphosphate aldolase, glyceraldehyde-3-phosphate dehydrogenase, phosphofructokinase, and phosphoglycerate kinase) were retained by the drug-affinity column (Table 1). As a result, we evaluated the possibility that CBL0137 affected ATP homeostasis since this nucleoside triphosphate is produced predominantly from glycolysis in bloodstream *T. brucei* (Brown et al., 2006; Schnaufer

et al., 2005; Van Weelden et al., 2003). CBL0137 did not affect cytosolic ATP levels whereas

control 2-deoxyglucose depleted the nucleotide (Fig. S1). We infer that CBL0137, although it

binds to some glycolytic enzymes (Table 1), is unlikely to inhibit their activity.

DNA-binding proteins replication protein A1 (RPA1), replication factor A2 (RPA2), and

universal minicircle sequence binding protein 2 (UMSBP2) were eluted with CBL0137 from the

drug-affinity column (Table 1). Homologs of RPA1 and RPA2 are part of a heterotrimeric

complex involved in DNA synthesis and damage response in other eukaryotes (Bochkarev et

al., 1999; Han et al., 2018; Haring et al., 2008; Kim and Brill, 2001; Olson et al., 2006). In *T.*

*brucei,* RPA2 is associated with nuclear DNA (Glover et al., 2019). Based on these facts we

hypothesized that CBL0137 might affect DNA replication and/or a DNA repair response.

**CBL0137 Inhibits DNA Synthesis and Nucleus Mitosis**

We tracked DNA replication in bloodstream *T. brucei* by monitoring incorporation of the

thymidine analog EdU into nuclear DNA. The effect of CBL0137 on DNA replication was

assessed by preincubating trypanosomes with the drug for 15 min before the addition of EdU for

1 h (Fig. 3). In absence of the drug robust DNA replication was documented in nuclei (Fig. 3A).

CBL0137 (180 nM) inhibited EdU incorporation into nuclei; median fluorescence dropped from

433 fluorescence units (FU) to 333.4 FU ($p = 2.2 \times 10^{-6}$ by Kolmogorov-Smirnov test) (Fig. 3B).

Higher amounts of CBL0137, $DCC_{50}$ (290 nM) and $DCC_{90}$ (800 nM), further reduced median

nuclear fluorescence to 152.7 FU and 82.3 FU, respectively ($p = 4.0 \times 10^{-6}$, and $p < 1 \times 10^{-15}$,

respectively) (Fig. 3B).

As control, we checked whether the synthesis of mitochondrial DNA (termed kinetoplast

DNA; kDNA) was affected by CBL0137. CBL0137 did not inhibit the replication of kDNA (Fig.

3C). So, we conclude that CBL0137 selectively inhibits nuclear DNA synthesis in *T. brucei.*

We reported in an earlier study that long-term exposure of trypanosomes to CBL0137

prevented mitosis of the nucleus (Thomas et al., 2016b). For that reason, we wanted to learn

whether short-term exposure of trypanosomes to CBL0137 prevented mitosis. To test whether

limited exposure of trypanosomes to CBL0137 affected mitosis, we treated cells (5 x $10^5$/ml)

with $DCC_{25}$ (180 nM), $DCC_{50}$ (290 nM) or $DCC_{90}$ (800 nM) drug for 6 h (Fig. 4) and then

analyzed the data. Trypanosomes with two kinetoplasts and one nucleus (2K1N) accumulated

after the 6 h treatment with CBL0137, and the fraction of 2K1N cells increased for $DCC_{50}$ (290

nM) as well as $DCC_{90}$ (800 nM) (Fig. 4). These data indicate that inhibition of mitosis is a major

effect of short-term treatment of bloodstream *T. brucei* with CBL0137.


**RPA1 and RPA2 are Physiologic Targets of CBL0137**

CBL0137 binds to multiple proteins (Table 1) many of which may not be the basis of the drug's

mode of action in a trypanosome. Physiological targets are a subset of drug-binding proteins

whose genetic knockdown (or overexpression in some cases) produces molecular effects

similar to those obtained when the drug is added to cells (Mensa-Wilmot, 2021). After identifying

fourteen CBL0137-binding proteins (Table 1) and learning that the drug does not block

glycolysis (Supp. Fig. S1) but inhibits DNA replication (Fig. 3), limits protein synthesis (Fig. 8),

and prevents mitosis (Fig. 4), we searched for physiological targets of the drug.

Since CBL0137 inhibited nuclear DNA replication (Fig. 3) we were interested in a

CBL0137-binding protein whose knockdown reduced DNA synthesis in the nucleus, as a

possible physiologic target of the drug. RPA1 is a single-stranded DNA binding protein that is

important for synthesis of DNA in other biological systems (Braun et al., 1997; Erdile et al.,

1991; Maniar et al., 1997; Mondal and Bhattacherjee, 2020) and other aspects of DNA

metabolism (reviewed in (Wold, 1997)). Trypanosome RPA1 is bound to CBL0137 (Table 1), so

we checked whether knockdown of RPA1 inhibited nuclear DNA synthesis. Towards this

objective, TbRPA1 was first tagged with a V5 epitope in a cell line where knockdown of the

gene could be induced with RNA interference. RPA1 was knocked down (Fig. 5A) resulting in a

2.5-fold reduction in protein level in an immunofluorescence assay (Fig. 5B) (p = $4.1 \times 10^{-5}$). A

control basal body protein TbRP2 was unaffected by RNAi of RPAi (Fig. 5C). Knockdown of

RPA1 was confirmed by western blotting (Supp. Fig. S3A, Supp. Fig. S4B) showing a seven-

fold reduction in protein amount (Supp. Fig. S3B) (p = 0.029). A trypanosome proliferation

defect was observed beginning 12 h after RNAi induction (Fig. S3C).

Regarding DNA replication, the fraction of EdU-positive trypanosomes decreased four-

fold (p = $1.8 \times 10^{-3}$) after the knockdown of RPA1 (Fig. 5E). Further, in the EdU-positive

population the amount of nucleotide analog incorporated decreased 350% (p < $1 \times 10^{-15}$) (Fig.

5F) after knockdown of TbRPA1. We conclude that RPA1 is important for DNA replication in *T.

brucei*.

Mitosis was inhibited after the knockdown of RPA1. The fraction of 2K1N cells increased

from 10% to 30% while 1K1N trypanosomes decreased from 80% to 45% (Fig. 5G). Further, we

detected XK1N trypanosomes that may have progressed from 2K1N trypanosomes. XK1N

trypanosomes duplicate kDNA multiple times without mitosis (Fig. 5G). Similarly, long-term

treatment of *T. brucei* with CBL0137 (200 nM for 24 h) produces XK1N cells (Thomas et al.,

2016b), in support of XK1N as a bona fide product of CBL0137 treatment of trypanosomes and

affirming a conclusion that knockdown of TbRPA1 phenocopies addition of the drug to *T. brucei*.

Our data is consistent with the conclusion that RPA1 is a physiologic target of CBL0137,

because knockdown of the gene phenocopies addition of the drug to *T. brucei* (Meyer and

Shapiro, 2021). Trypanosome RPA is a CBL0137-binding protein (Table 1) whose knockdown

inhibits DNA replication (Fig. 5F), and prevents mitosis (Fig. 5G), like results obtained after the

addition of CBL0137 to *T. brucei* (Fig. 3 and Fig. 4).

RPA2 is a CBL0137-binding protein (Table 1), so we determined whether it's genetic

knockdown inhibited DNA replication, mitosis or protein synthesis to find out whether the protein

was a physiologic target of the drug. RPA2 knockdown was engineered in a trypanosome line

expressing a myc-tagged version of the protein. Induction of RNAi reduced protein level four-

fold (Fig. 6A compare lane 3 to lane 4, and Fig. 6B), and proliferation of trypanosomes was

reduced 24 h after knockdown of RPA2 (Fig. 6C). The fraction of 2K1N trypanosomes rose from 10% to 20% after RNAi against RPA2 (Fig. 6D; p = 4.87 x 10$^{-29}$) indicating that mitosis was blocked. In addition, anucleate (1K0N) trypanosomes accumulated in the population (Fig. 6D; Supp. Fig. S4). (Bloodstream trypanosomes in G1 have one kinetoplast (K) and one nucleus (N) (1K1N). Anucleate cells, also termed zoids, have a kinetoplast but lack a nucleus (1K0N).) CBL0137 treatment of *T. brucei* does not produce anucleate cells (Fig. 4).

These data imply that knockdown of RPA2 protein partially phenocopies addition of CBL0137 to trypanosomes and is consistent with RPA2 as a physiological target of CBL0137. This inference is in line with polypharmacology of the drug in *T. brucei*. Our finding that RPA2 is important for accurate partitioning of the nucleus is a novel observation.


**UMSBP2 is Not a Physiological Target for CBL0137**

UMSBP2 binds mitochondrial DNA (termed kinetoplast DNA (kDNA) as well as telomeres of nuclear DNA (Jensen and Englund, 2012; Klebanov-Akopyan et al., 2018; Povelones, 2014). Since UMSBP2 is a CBL0137-binding protein (Table 1), we were interested in learning whether knockdown of UMSBP2 phenocopied CBL0137 by inhibiting mitosis, reducing DNA synthesis, or blocking protein synthesis, as expected for a physiologic target (Meyer and Shapiro, 2021).

UMSBP2 knockdown (Fig. 7A) reduced protein amount six-fold (Fig. 7B) and slowed proliferation after 36 h (Fig. 7C). Phenotypically, there was a slight increase in 1K1N cells accompanied by a decrease in 2K1N cells (Fig. 7D) but the difference in distribution of cell types was not statistically significant (p = 0.1514). Further, this change in the distribution of cells was not reproduced in a second knockdown line. We conclude that knockdown of UMSBP2 has a minor effect on the proliferation of bloodstream *T. brucei*, unlike the situation in insect stage (procyclic) *T. brucei* where mitosis or kDNA segregation were affected (Klebanov-Akopyan et al., 2018; Milman et al., 2007). In bloodstream *T. brucei* knockdown of UMSBP2 did not inhibit mitosis (Fig. 7). Thus, although UMSBP2 is a CBL0137-binding protein (Table 1) it is not a

physiologic target of the drug, because it's knockdown does not phenocopy molecular effects of adding CBL0137 to trypanosomes. The caveat in interpretation of this data is the assumption that association of CBL0137 with UMSBP2 causes inhibition of the protein's activity. If CBL0137 activated UMSBP2 the appropriate study will be overexpression of the protein (discussed in (Mensa-Wilmot, 2021)).


**Proteostasis of Epitope-Tagged Polypeptides is Perturbed by CBL0137**

Trypanosomes are not viable after a 6-h treatment with CBL0137 (Fig. 1). From that observation we hypothesized that CBL0137 exerted an irreversible cidal effect on bloodstream *T. brucei*. Since TbRPA1 emerged as a physiologic target of CBL0137 (see the last section), we hypothesized that exposure of *T. brucei* to CBL0137 caused irreversible loss of RPA1 protein from the cells. To test our hypothesis, we tagged RPA1 with a V5 epitope on the N-terminus, obtained stable transfectants, and treated that *T. brucei* line with CBL0137 (720 nM; $DCC_{90}$) for 6 h (Fig. 8A). Cells were analyzed by western blotting for V5-RPA1 protein before and after drug exposure (Fig. 8B). Total protein in each lane was quantitated with a "stain-free" dye (see Materials and Methods) (Gilda and Gomes, 2015; Gurtler et al., 2013) (Fig. 8C) and that data was used to normalize the anti-V5 antibody signal (Fig. 8D).

CBL0137 reduced the amount of RPA1 by fifty percent (compare DMSO to CBL0137-treated samples, respectively lane 2 to and lane 3 of Fig. 8B) after a 6 h treatment of *T. brucei* with the drug (Fig. 8D) ($p = 2.3 \times 10^{-3}$). In a set of control experiments, we checked the effect of CBL0137 on steady-state levels of NRP1 and Tb427.03.1010, using an approach like that described for RPA1. Steady-state amounts of both NRP1 (Fig. 8B lanes 4, 5 and 6; Fig. 8D) and Tb427.03.1010 (Fig. 8B lanes 7, 8 and 9; Fig. 8D) decreased 50% under similar circumstances. We conclude that CBL0137 reduces steady-state amounts of V5-tagged RPA1, NRP1 and Tb427.03.1010, indicating that the effect of the drug was not limited to RPA1. Thus, CBL0137 either causes proteolysis of the three proteins in this study, or triggers digestion of most

trypanosome proteins. (Possible effects of the drug on polypeptide synthesis is addressed in the next section.)

We examined a hypothesis that CBL0137 caused digestion of most proteins after trypanosome exposure to the drug. For this purpose, total protein used for western blots (Fig. 7) ($10^6$ cell equivalents per lane) was quantitated using TGX Fast-Cast$^{TM}$ Stain-free, and fluorescence images acquired with a ChemiDoc XRS+ system (Bio-Rad) (see Materials and Methods) (Supp. Fig. S6A). Differences in total protein amounts before and after CBL0137 treatment (6 h) was not statistically significant between the two conditions (Supp. Fig. S6B). Thus, CBL0137 does not trigger mass degradation of proteins in *T. brucei*. Instead, proteolysis induced by CBL0137 affects the three proteins that we tracked (Fig. 8). A trivial explanation for these data is that the V5 epitope on the three proteins marked them for degradation in presence of CBL0137. This hypothesis was tested by comparing three tags (V5, HA and Myc) each appended separately to the c-terminus of a single protein TbCK1.2 (Supp. Fig. S6C). Degradation of the three versions of TbCK1.2 was monitored as described for the proteins presented earlier (Fig. 8). CBL0137 addition to trypanosomes harboring these constructs led to loss of all three proteins (Supp. Fig. S6C). Altogether the data indicates that CBL0137 causes degradation of some but not all proteins. Further work is needed to examine this effect in detail.

**CBL0137 Blocks Protein Synthesis**

Our observation that CBL0137 reduces abundance of several proteins (Fig. 8) led us to explore a possibility that the drug affected either (i) degradation and/or (ii) synthesis of proteins. To distinguish between these possibilities, we examined the effect of CBL0137 on ribosomal protein synthesis, tracked by incorporation of a methionine analog L-homopropargylglycine (HPG) into polypeptides (Landgraf et al., 2015) (Fig. 9A).

Trypanosome polypeptides incorporate HPG (Fig. 9B, lane 2), and the process was blocked by cycloheximide, an inhibitor of eukaryote protein synthesis (Duszenko et al., 1999;

Siegel et al., 2008) (Fig. 9B, lane 3). Effect of CBL0137 (180 nM ($DCC_{25}$), 290 nM ($DCC_{50}$), or

800 nM ($DCC_{90}$) on translation was assayed by a 15 min preincubation of cells with drug

followed by addition of HPG for 60 min (Fig. 9B, lane 4, lane 5 and lane 6). HPG incorporation

into polypeptide was normalized to total protein content (Fig. 9B lanes 7-12). CBL0137 inhibited

translation at 290 nM ($DCC_{50}$) ($p = 3 \times 10^{-2}$), and 800 nM ($DCC_{90}$) ($p = 2 \times 10^{-3}$), but not at 180

nM ($DCC_{25}$) (Fig. 9C).

We surmise that CBL0137 inhibits translation of trypanosome proteins, an observation

that helps explain reduction in steady-state amount of four proteins studied earlier (Fig. 8; Supp.

Fig. S6C). If new protein synthesis is inhibited by CBL0137 (Fig. 9) polypeptides with short half-

lives may not be replenished when trypanosomes are treated with drug for 6 h, leading to

diminished steady-state levels in western blot assays (Fig. 8, Supp. Fig. S6). Efficacy of

CBL0137 against *T. brucei* in a mouse model of HAT (Thomas et al., 2016b) most likely

involves inhibition of protein synthesis, because plasma concentration of CBL0137 reaches 1.7

μM after oral administration of drug (40 mg/kg) (Sharma *et. al.,* in preparation). RPA1

knockdown, while copying some molecular effects of CBL0137, does not inhibit translation of

proteins in *T. brucei* (Supp. Fig. S5).

## DISCUSSION

### From Binding-Proteins to Physiologic Targets of Drugs

Implementation of "phenotypic screening" is on the rise in drug discovery projects for infectious, parasitic, oncologic, and chronic diseases (Bachovchin et al., 2019; Bryce et al., 2019; Buckner et al., 2020; Chatelain and Ioset, 2018; Ferrins et al., 2018; Love and McNamara, 2021; Patra et al., 2020; Vincent et al., 2020; Warchal et al., 2020; Woodring et al., 2018). Since targets of drugs discovered by phenotypic screening are unknown, an effort to find drug-binding proteins is a typical next step to understand mechanisms of action of the new drugs.

While many pathways for drug target deconvolution are available, the most convincing ones use assays that are (a) unbiased, and (b) monitor direct biochemical interactions between drugs and binding proteins (*e.g.,* affinity chromatography, and photo-affinity labeling) (Franks and Hsu, 2019; Rix et al., 2007; Shi et al., 2012). Such direct strategies frequently yield tens of drug-binding proteins (Jones et al., 2015), creating a need to distinguish drug-binding proteins from physiologic targets of drugs. A "physiologic target of a drug" may be defined as a macromolecule whose knockdown or over-expression produces identical (or very similar) molecular effects as treatment of cells with the drug (Mensa-Wilmot, 2021). Many drug-binding proteins, for example, plasma proteins (Berezhkovskiy, 2008; Cho et al., 2010; Svennebring, 2016), are not physiological targets of the small molecules.

### CBL0137-binding proteins and Molecular Modes of Action of the Drug

Fourteen CBL0137-binding proteins were identified with affinity chromatography (Table 1) and were used to predict molecular effects of CBL0137 on trypanosomes exposed to pharmacodynamically equivalent drug concentrations ($DCC_{25}$, for example) (Fig. 1).

CBL0137 inhibited nuclear (but not mitochondrial) DNA replication (Fig. 3), prevented nucleus mitosis (Fig. 4) and blocked polypeptide synthesis (Fig. 9). Despite identification of

several glycolysis enzymes as drug-binding proteins (Table 1), CBL0137 failed to inhibit ATP synthesis (Supp. Fig. S1), indicating that those enzymes are unlikely to be physiologic targets of the drug.

CBL0137 inhibition of polypeptide synthesis (Fig. 9) could explain pleiotropy of the drug's molecular effects. For example, blocking translation of proteins with short half-lives may be equivalent to a "loss of function" that leads to a specific molecular defect (*e.g.,* inhibition of DNA synthesis). However, that hypothesis is undercut by the use of less drug to inhibit both DNA synthesis and mitosis than is needed to block translation (Fig. 9). Several antibacterial drugs act on ribosomal protein synthesis (reviewed in (Lin et al., 2018)). In trypanosomes, no inhibitors of protein synthesis are currently in development as drugs against the pathogen, although small molecules that inhibit methionyl-tRNA synthetase are being optimized (Huang et al., 2016; Zhang et al., 2020). To that end, CBL0137 represents a "first in class" lead drug with protein synthesis as a mode of action. CBL0137 is the first carbazole inhibitor of eukaryote protein synthesis.

In a previous study, a 24-h treatment of *T. brucei* with 200 nM CBL0137 did not inhibit DNA synthesis (Thomas et al., 2016b), apparently contradicting data presented in Fig. 3 of this work. In experiments to resolve this discrepancy, we found that in a 6-h treatment of *T. brucei* it requires 730 nM CBL0137 to inhibit DNA synthesis (Supp. Fig. S2). A simple explanation for the observation is that a lower amount of CBL0137 slows down but does not terminate DNA synthesis thereby permitting DNA replication over a long period of time. Curiously, the higher concentration of drug needed to inhibit DNA synthesis is exceeded in mice after oral dosing (60 mg/kg) of CBL0137 (Sharma *et al.*, in preparation). Therefore, it seems possible that the trypanocidal effect of CBL0137 in mice involves inhibition of nuclear DNA synthesis.

Polypharmacology of CBL0137 (*i.e.*, inhibition of DNA replication, mitosis, and protein synthesis at concentrations above 290 nM) (Fig. 10) bodes well for using it as an anti-

trypanosome drug. Interaction with two or more targets suggests that it might be difficult for trypanosomes to develop resistance after chemotherapy with CBL0137.

**Physiologic Targets Explain Modes of Action of CBL0137**

We used affinity chromatography, as an unbiased approach, to identify fourteen CBL0137-binding proteins (Table 1). These CBL0137-binding proteins may seem unique when compared to the data from human cells, where the drug interferes with aspects of chromatin biology (Dallavalle et al., 2021; Lu et al., 2021; Sergeev et al., 2020). However, no CBL0137-binding proteins have been identified with an unbiased biochemical strategy in human cells. Therefore, one cannot directly compare our data with information from human cells.

In pursuit of physiologic targets of the drug, trypanosome genes encoding CBL0137-binding proteins were knocked down, and resulting molecular effects were compared to those obtained after perturbation of trypanosomes with the drug (Meyer and Shapiro, 2021). For physiologic targets of the drug, the expectation was that molecular defects determined after their knockdown would be very similar to those obtained after adding CBL0137 to trypanosomes (Mensa-Wilmot, 2021).

Data obtained for RPA1 and RPA2 is consistent with their designation as physiologic targets of CBL0137. Knockdown of that RPA1 inhibited DNA replication, and prevented mitosis, like effects observed after adding CBL0137 to trypanosomes. RPA2, expected to form a complex with RPA1 *in vivo* (Chen and Wold, 2014; Maniar et al., 1997), yielded data after RNAi that are in line with designation as a physiologic target, by inhibiting mitosis (Fig. 6D). That knockdown of RPA1 and RPA2 did not produce identical results in *T. brucei* is not completely surprising since divergence of the functions of RPA1 and RPA2 has been noted in *A. thaliana* and in *C. elegans* (Hefel et al., 2021).

Involvement of RPA1 in mitosis is novel. In other organisms, homologs of the protein in complex with RPA2 and RPA3 participate in aspects of DNA synthesis, repair, and

recombination (Caldwell and Spies, 2020; Chowdhury et al., 2021). However, there are no reports yet of a role in mitosis. In future work, analysis of the binding partners of trypanosome RPA1 may shed light on how the protein contributes to mitosis.

Further work is needed to identify other physiologic targets of CBL0137. We do not know proteins whose interaction with CBL0137 inhibits translation of mRNAs (Fig. 9). Our affinity chromatography work produced four RNA-binding proteins, namely Poly(A)-binding protein 2 (PABP 2), an ALBA-domain protein, RNA-binding protein DRBD2, and RNA-binding protein DRBD3 as CBL0137-binding proteins (Table 1). These genes will be a good starting point to discover physiologic targets of CBL0137 that regulate protein synthesis in the African trypanosome.

**ACKNOWLEDGEMENTS**

**ACKNOWLEDGEMENTS**

**Authorship Contributions.**

*Participated in research design:* Mensa-Wilmot, Sanz-Rodríguez, Guyett

*Conducted experiments:* Sanz-Rodríguez, Hoffman

*Contributed new reagents or analytic tools:* Guyett, Singh, Pollastri

*Performed data analysis:* Sanz-Rodríguez, Hoffman, Mensa-Wilmot

*Wrote or contributed to the writing of the manuscript:* Mensa-Wilmot, Pollastri, Purmal, Hoffman

LITERATURE CITED

Abo-Rady M, Bellmann J, Glatza M, Marrone L, Reinhardt L, Tena S and Sterneckert J (2019) Phenotypic Screening Using Mouse and Human Stem Cell-Based Models of Neuroinflammation and Gene Expression Analysis to Study Drug Responses. *Methods Mol Biol* **1888**: 21-43.

Andre J, Kerry L, Qi X, Hawkins E, Drizyte K, Ginger ML and McKean PG (2014) An alternative model for the role of RP2 protein in flagellum assembly in the African trypanosome. *J Biol Chem* **289**(1): 464-475.

Bachovchin KA, Sharma A, Bag S, Klug DM, Schneider KM, Singh B, Jalani HB, Buskes MJ, Mehta N, Tanghe S, Momper JD, Sciotti RJ, Rodriguez A, Mensa-Wilmot K, Pollastri MP and Ferrins L (2019) Improvement of Aqueous Solubility of Lapatinib-Derived Analogues: Identification of a Quinolinimine Lead for Human African Trypanosomiasis Drug Development. *Journal of Medicinal Chemistry* **62**(2): 665-687.

Berezhkovskiy LM (2008) Some features of the kinetics and equilibrium of drug binding to plasma proteins. *Expert opinion on drug metabolism & toxicology* **4**(12): 1479-1498.

Bochkarev A, Bochkareva E, Frappier L and Edwards AM (1999) The crystal structure of the complex of replication protein A subunits RPA32 and RPA14 reveals a mechanism for single-stranded DNA binding. *EMBO J* **18**(16): 4498-4504.

Braun KA, Lao Y, He Z, Ingles CJ and Wold MS (1997) Role of protein-protein interactions in the function of replication protein A (RPA): RPA modulates the activity of DNA polymerase alpha by multiple mechanisms. *Biochemistry* **36**(28): 8443-8454.

Brown SV, Hosking P, Li J and Williams N (2006) ATP synthase is responsible for maintaining mitochondrial membrane potential in bloodstream form Trypanosoma brucei. *Eukaryot Cell* **5**(1): 45-53.

Bryce NS, Hardeman EC, Gunning PW and Lock JG (2019) Chemical biology approaches targeting the actin cytoskeleton through phenotypic screening. *Curr Opin Chem Biol* **51**: 40-47.

Buckner FS, Buchynskyy A, Nagendar P, Patrick DA, Gillespie JR, Herbst Z, Tidwell RR and Gelb MH (2020) Phenotypic Drug Discovery for Human African Trypanosomiasis: A Powerful Approach. *Trop Med Infect Dis* **5**(1).

Butera JA (2013) Phenotypic screening as a strategic component of drug discovery programs targeting novel antiparasitic and antimycobacterial agents: an editorial. *J Med Chem* **56**(20): 7715-7718.

Caldwell CC and Spies M (2020) Dynamic elements of replication protein A at the crossroads of DNA replication, recombination, and repair. *Crit Rev Biochem Mol Biol* **55**(5): 482-507.

Chatelain E and Ioset JR (2018) Phenotypic screening approaches for Chagas disease drug discovery. *Expert opinion on drug discovery* **13**(2): 141-153.

Chen R and Wold MS (2014) Replication protein A: single-stranded DNA's first responder: dynamic DNA-interactions allow replication protein A to direct single-strand DNA intermediates into different pathways for synthesis or repair. *Bioessays* **36**(12): 1156-1161.

Cho SY, Ohnuma T, Silverman LR, Holland JF and Roboz J (2010) Discontinuous drug binding to proteins: binding of an antineoplastic benzyl styryl sulfone to albumin and enzymes in vitro and in phase I clinical trials. *Drug metabolism and disposition: the biological fate of chemicals* **38**(9): 1480-1485.

Chowdhury S, Chowdhury AB, Kumar M and Chakraborty S (2021) Revisiting regulatory roles of replication protein A in plant DNA metabolism. *Planta* **253**(6): 130.

Dallavalle S, Mattio LM, Artali R, Musso L, Avino A, Fabrega C, Eritja R, Gargallo R and Mazzini S (2021) Exploring the Interaction of Curaxin CBL0137 with G-Quadruplex DNA Oligomers. *International journal of molecular sciences* **22**(12).

Drowley L, McPheat J, Nordqvist A, Peel S, Karlsson U, Martinsson S, Mullers E, Dellsen A, Knight S, Barrett I, Sanchez J, Magnusson B, Greber B, Wang QD and Plowright AT (2020) Discovery of retinoic acid receptor agonists as proliferators of cardiac progenitor cells through a phenotypic screening approach. *Stem cells translational medicine* **9**(1): 47-60.

Duszenko M, Kang X, Bohme U, Homke R and Lehner M (1999) In vitro translation in a cell-free system from Trypanosoma brucei yields glycosylated and glycosylphosphatidylinositol-anchored proteins. *Eur J Biochem* **266**(3): 789-797.

Eng JK, McCormack AL and Yates JR (1994) An approach to correlate tandem mass spectral data of peptides with amino acid sequences in a protein database. *J Am Soc Mass Spectrom* **5**(11): 976-989.

Erdile LF, Heyer WD, Kolodner R and Kelly TJ (1991) Characterization of a cDNA encoding the 70-kDa single-stranded DNA-binding subunit of human replication protein A and the role of the protein in DNA replication. *J Biol Chem* **266**(18): 12090-12098.

Ferguson L, Wells G, Bhakta S, Johnson J, Guzman J, Parish T, Prentice RA and Brucoli F (2019) Integrated Target-Based and Phenotypic Screening Approaches for the Identification of Anti-Tubercular Agents That Bind to the Mycobacterial Adenylating Enzyme MbtA. *ChemMedChem* **14**(19): 1735-1741.

Ferrins L, Sharma A, Thomas SM, Mehta N, Erath J, Tanghe S, Leed SE, Rodriguez A, Mensa-Wilmot K, Sciotti RJ, Gillingwater K and Pollastri MP (2018) Anilinoquinoline based inhibitors of trypanosomatid proliferation. *PLOS Neglected Tropical Diseases* **12**(11): e0006834.

Franks CE and Hsu KL (2019) Activity-Based Kinome Profiling Using Chemical Proteomics and ATP Acyl Phosphates. *Current protocols in chemical biology* **11**(3): e72.

Gilda JE and Gomes AV (2015) Western blotting using in-gel protein labeling as a normalization control: stain-free technology. *Methods Mol Biol* **1295**: 381-391.

Glover L, Marques CA, Suska O and Horn D (2019) Persistent DNA Damage Foci and DNA Replication with a Broken Chromosome in the African Trypanosome. *mBio* **10**(4).

Gurtler A, Kunz N, Gomolka M, Hornhardt S, Friedl AA, McDonald K, Kohn JE and Posch A (2013) Stain-Free technology as a normalization tool in Western blot analysis. *Anal Biochem* **433**(2): 105-111.

Guyett PJ, Xia S, Swinney DC, Pollastri MP and Mensa-Wilmot K (2016) Glycogen Synthase Kinase 3beta Promotes the Endocytosis of Transferrin in the African Trypanosome. *ACS Infect Dis* **2**(7): 518-528.

Han JJ, Song ZT, Sun JL, Yang ZT, Xian MJ, Wang S, Sun L and Liu JX (2018) Chromatin remodeling factor CHR18 interacts with replication protein RPA1A to regulate the DNA replication stress response in Arabidopsis. *New Phytol* **220**(2): 476-487.

Haring SJ, Mason AC, Binz SK and Wold MS (2008) Cellular functions of human RPA1. Multiple roles of domains in replication, repair, and checkpoints. *J Biol Chem* **283**(27): 19095-19111.

Hefel A, Honda M, Cronin N, Harrell K, Patel P, Spies M and Smolikove S (2021) RPA complexes in Caenorhabditis elegans meiosis; unique roles in replication, meiotic recombination and apoptosis. *Nucleic Acids Res* **49**(4): 2005-2026.

Hirumi H and Hirumi K (1989) Continuous cultivation of Trypanosoma brucei blood stream forms in a medium containing a low concentration of serum protein without feeder cell layers. *J Parasitol* **75**(6): 985-989.

Huang W, Zhang Z, Barros-Alvarez X, Koh CY, Ranade RM, Gillespie JR, Creason SA, Shibata S, Verlinde C, Hol WGJ, Buckner FS and Fan E (2016) Structure-guided design of novel Trypanosoma brucei Methionyl-tRNA synthetase inhibitors. *Eur J Med Chem* **124**: 1081-1092.

Jacobs RT, Plattner JJ, Nare B, Wring SA, Chen D, Freund Y, Gaukel EG, Orr MD, Perales JB, Jenks M, Noe RA, Sligar JM, Zhang YK, Bacchi CJ, Yarlett N and Don R (2011) Benzoxaboroles: a new class of potential drugs for human African trypanosomiasis. *Future medicinal chemistry* **3**(10): 1259-1278.

Jensen RE and Englund PT (2012) Network news: the replication of kinetoplast DNA. *Annual review of microbiology* **66**: 473-491.

Jones DC, Foth BJ, Urbaniak MD, Patterson S, Ong HB, Berriman M and Fairlamb AH (2015) Genomic and Proteomic Studies on the Mode of Action of Oxaboroles against the African Trypanosome. *PLoS Negl Trop Dis* **9**(12): e0004299.

Kaiser M, Bray MA, Cal M, Bourdin Trunz B, Torreele E and Brun R (2011) Antitrypanosomal activity of fexinidazole, a new oral nitroimidazole drug candidate for treatment of sleeping sickness. *Antimicrob Agents Chemother* **55**(12): 5602-5608.

Kall L, Canterbury JD, Weston J, Noble WS and MacCoss MJ (2007) Semi-supervised learning for peptide identification from shotgun proteomics datasets. *Nat Methods* **4**(11): 923-925.

Kall L, Storey JD and Noble WS (2008) Non-parametric estimation of posterior error probabilities associated with peptides identified by tandem mass spectrometry. *Bioinformatics* **24**(16): i42-48.

Kall L, Storey JD and Noble WS (2009) QVALITY: non-parametric estimation of q-values and posterior error probabilities. *Bioinformatics* **25**(7): 964-966.

Keatinge M, Tsarouchas TM, Munir T, Porter NJ, Larraz J, Gianni D, Tsai HH, Becker CG, Lyons DA and Becker T (2021) CRISPR gRNA phenotypic screening in zebrafish reveals pro-regenerative genes in spinal cord injury. *PLoS genetics* **17**(4): e1009515.

Kim HS and Brill SJ (2001) Rfc4 interacts with Rpa1 and is required for both DNA replication and DNA damage checkpoints in Saccharomyces cerevisiae. *Mol Cell Biol* **21**(11): 3725-3737.

Klebanov-Akopyan O, Mishra A, Glousker G, Tzfati Y and Shlomai J (2018) Trypanosoma brucei UMSBP2 is a single-stranded telomeric DNA binding protein essential for chromosome end protection. *Nucleic Acids Res* **46**(15): 7757-7771.

Koman IE, Commane M, Paszkiewicz G, Hoonjan B, Pal S, Safina A, Toshkov I, Purmal AA, Wang D, Liu S, Morrison C, Gudkov AV and Gurova KV (2012) Targeting FACT complex suppresses mammary tumorigenesis in Her2/neu transgenic mice. *Cancer prevention research* **5**(8): 1025-1035.

Landgraf P, Antileo ER, Schuman EM and Dieterich DC (2015) BONCAT: metabolic labeling, click chemistry, and affinity purification of newly synthesized proteomes. *Methods Mol Biol* **1266**: 199-215.

Lin J, Zhou D, Steitz TA, Polikanov YS and Gagnon MG (2018) Ribosome-Targeting Antibiotics: Modes of Action, Mechanisms of Resistance, and Implications for Drug Design. *Annu Rev Biochem* **87**: 451-478.

Lindner AK, Lejon V, Chappuis F, Seixas J, Kazumba L, Barrett MP, Mwamba E, Erphas O, Akl EA, Villanueva G, Bergman H, Simarro P, Kadima Ebeja A, Priotto G and Franco JR (2020) New WHO guidelines for treatment of gambiense human African trypanosomiasis including fexinidazole: substantial changes for clinical practice. *Lancet Infect Dis* **20**(2): e38-e46.

Love MS and McNamara CW (2021) Phenotypic screening techniques for Cryptosporidium drug discovery. *Expert opinion on drug discovery* **16**(1): 59-74.

Lu K, Liu C, Liu Y, Luo A, Chen J, Lei Z, Kong J, Xiao X, Zhang S, Wang YZ, Ma L, Dou SX, Wang PY, Li M, Li G, Li W and Chen P (2021) Curaxin-Induced DNA Topology Alterations Trigger the Distinct Binding Response of CTCF and FACT at the Single-Molecule Level. *Biochemistry* **60**(7): 494-499.

Maniar HS, Wilson R and Brill SJ (1997) Roles of replication protein-A subunits 2 and 3 in DNA replication fork movement in Saccharomyces cerevisiae. *Genetics* **145**(4): 891-902.

McQuin C, Goodman A, Chernyshev V, Kamentsky L, Cimini BA, Karhohs KW, Doan M, Ding L, Rafelski SM, Thirstrup D, Wiegraebe W, Singh S, Becker T, Caicedo JC and Carpenter AE (2018) CellProfiler 3.0: Next-generation image processing for biology. *PLoS Biol* **16**(7): e2005970.

Mensa-Wilmot K (2021) How Physiologic Targets Can Be Distinguished from Drug-Binding Proteins. *Mol Pharmacol* **100**(1): 1-6.

Meyer KJ and Shapiro TA (2021) Cytosolic and Mitochondrial Hsp90 in Cytokinesis, Mitochondrial DNA Replication, and Drug Action in Trypanosoma brucei. *Antimicrob Agents Chemother* **65**(11): e0063221.

Milman N, Motyka SA, Englund PT, Robinson D and Shlomai J (2007) Mitochondrial origin-binding protein UMSBP mediates DNA replication and segregation in trypanosomes. *Proc Natl Acad Sci U S A* **104**(49): 19250-19255.

Mondal A and Bhattacherjee A (2020) Mechanism of Dynamic Binding of Replication Protein A to ssDNA. *J Chem Inf Model* **60**(10): 5057-5069.

Olson E, Nievera CJ, Klimovich V, Fanning E and Wu X (2006) RPA2 is a direct downstream target for ATR to regulate the S-phase checkpoint. *J Biol Chem* **281**(51): 39517-39533.

Orsburn BC (2021) Proteome Discoverer-A Community Enhanced Data Processing Suite for Protein Informatics. *Proteomes* **9**(1).

Palomba A, Abbondio M, Fiorito G, Uzzau S, Pagnozzi D and Tanca A (2021) Comparative Evaluation of MaxQuant and Proteome Discoverer MS1-Based Protein Quantification Tools. *J Proteome Res* **20**(7): 3497-3507.

Patra AT, Hingamire T, Belekar MA, Xiong A, Subramanian G, Bozdech Z, Preiser P, Shanmugam D and Chandramohanadas R (2020) Whole-Cell Phenotypic Screening of Medicines for Malaria Venture Pathogen Box Identifies Specific Inhibitors of Plasmodium falciparum Late-Stage Development and Egress. *Antimicrob Agents Chemother* **64**(5).

Pelfrene E, Harvey Allchurch M, Ntamabyaliro N, Nambasa V, Ventura FV, Nagercoil N and Cavaleri M (2019) The European Medicines Agency's scientific opinion on oral fexinidazole for human African trypanosomiasis. *PLoS Negl Trop Dis* **13**(6): e0007381.

Pollastri MP (2018) Fexinidazole: a new drug for African sleeping sickness on the horizon. *Trends in Parasitology* **34**(3): 178-179.

Povelones ML (2014) Beyond replication: Division and segregation of mitochondrial DNA in kinetoplastids. *Mol Biochem Parasitol*.

Punna S, Kaltgrad E and Finn MG (2005) "Clickable" agarose for affinity chromatography. *Bioconjug Chem* **16**(6): 1536-1541.

Rix U, Hantschel O, Durnberger G, Remsing Rix LL, Planyavsky M, Fernbach NV, Kaupe I, Bennett KL, Valent P, Colinge J, Kocher T and Superti-Furga G (2007) Chemical proteomic profiles of the BCR-ABL inhibitors imatinib, nilotinib, and dasatinib reveal novel kinase and nonkinase targets. *Blood* **110**(12): 4055-4063.

Rostovtsev VV, Green LG, Fokin VV and Sharpless KB (2002) A stepwise huisgen cycloaddition process: copper(I)-catalyzed regioselective "ligation" of azides and terminal alkynes. *Angew Chem Int Ed Engl* **41**(14): 2596-2599.

Ruillier V, Tournois J, Boissart C, Lasbareilles M, Mahe G, Chatrousse L, Cailleret M, Peschanski M and Benchoua A (2020) Rescuing compounds for Lesch-Nyhan disease identified using stem cell-based phenotypic screening. *JCI Insight* **5**(4).

Schnaufer A, Clark-Walker GD, Steinberg AG and Stuart K (2005) The F1-ATP synthase complex in bloodstream stage trypanosomes has an unusual and essential function. *EMBO J* **24**(23): 4029-4040.

Sergeev A, Vorobyov A, Yakubovskaya M, Kirsanova O and Gromova E (2020) Novel anticancer drug curaxin CBL0137 impairs DNA methylation by eukaryotic DNA methyltransferase Dnmt3a. *Bioorg Med Chem Lett* **30**(16): 127296.

Shapovalov V, Kopanitsa L, Pruteanu LL, Ladds G and Bailey DS (2021) Transcriptomics-Based Phenotypic Screening Supports Drug Discovery in Human Glioblastoma Cells. *Cancers (Basel)* **13**(15).

Shen S, Arhun, G., Ullu, E., Tschudi, C. (2001) In vivo epitope tagging of Trypanosoma brucei genes using a one step PCR-based strategy. *Molecular and Biochemical Parasitology* **113**: 171-173.

Shi H, Zhang CJ, Chen GY and Yao SQ (2012) Cell-based proteome profiling of potential dasatinib targets by use of affinity-based probes. *J Am Chem Soc* **134**(6): 3001-3014.

Siegel TN, Kawahara T, Degrasse JA, Janzen CJ, Horn D and Cross GA (2008) Acetylation of histone H4K4 is cell cycle regulated and mediated by HAT3 in Trypanosoma brucei. *Mol Microbiol* **67**(4): 762-771.

Sokolova AY, Wyllie S, Patterson S, Oza SL, Read KD and Fairlamb AH (2010) Cross-resistance to nitro drugs and implications for treatment of human African trypanosomiasis. *Antimicrob Agents Chemother* **54**(7): 2893-2900.

Soliman K (2015) CellProfiler: Novel Automated Image Segmentation Procedure for Super-Resolution Microscopy. *Biol Proced Online* **17**: 11.

Sullenberger C, Pique D, Ogata Y and Mensa-Wilmot K (2017) AEE788 Inhibits Basal Body Assembly and Blocks DNA Replication in the African Trypanosome. *Mol Pharmacol* **91**(5): 482-498.

Svennebring AM (2016) The impact of the concentration of drug binding plasma proteins on drug distribution according to Oie-Tozer's model. *Xenobiotica; the fate of foreign compounds in biological systems* **46**(4): 307-314.

Swalley SE (2020) Expanding therapeutic opportunities for neurodegenerative diseases: A perspective on the important role of phenotypic screening. *Bioorg Med Chem* **28**(3): 115239.

Swinney DC and Anthony J (2011) How were new medicines discovered? *Nature reviews Drug discovery* **10**(7): 507-519.

Thomas SM, Purmal A, Pollastri M and Mensa-Wilmot K (2016a) Discovery of a Carbazole-Derived Lead Drug for Human African Trypanosomiasis. *Sci Rep* **6**: 32083.

Thomas SM, Purmal A, Pollastri M and Mensa-Wilmot K (2016b) Discovery of a carbazole-derived lead drug for human African trypanosomiasis. *Scientific Reports* **6**: 32083.

Torreele E, Bourdin Trunz B, Tweats D, Kaiser M, Brun R, Mazue G, Bray MA and Pecoul B (2010) Fexinidazole--a new oral nitroimidazole drug candidate entering clinical development for the treatment of sleeping sickness. *PLoS Negl Trop Dis* **4**(12): e923.

Van Weelden SW, Fast B, Vogt A, Van Der Meer P, Saas J, Van Hellemond JJ, Tielens AG and Boshart M (2003) Procyclic Trypanosoma brucei do not use Krebs cycle activity for energy generation. *J Biol Chem*.

Vincent F, Loria PM, Weston AD, Steppan CM, Doyonnas R, Wang YM, Rockwell KL and Peakman MC (2020) Hit Triage and Validation in Phenotypic Screening: Considerations and Strategies. *Cell Chem Biol* **27**(11): 1332-1346.

Wang F, Zhao Q, Liu J, Wang Z and Kong D (2020) Identification of human lactate dehydrogenase A inhibitors with anti-osteosarcoma activity through cell-based phenotypic screening. *Bioorg Med Chem Lett* **30**(4): 126909.

Warchal SJ, Dawson JC, Shepherd E, Munro AF, Hughes RE, Makda A and Carragher NO (2020) High content phenotypic screening identifies serotonin receptor modulators with selective activity upon breast cancer cell cycle and cytokine signaling pathways. *Bioorg Med Chem* **28**(1): 115209.

Watson JA, Strub-Wourgraft N, Tarral A, Ribeiro I, Tarning J and White NJ (2019) A pharmacokinetic-pharmacodynamic assessment of the hepatic and bone-marrow toxicities of the new trypanoside fexinidazole. *Antimicrob Agents Chemother*.

Weng Q, Che J, Zhang Z, Zheng J, Zhan W, Lin S, Tian T, Wang J, Gai R, Hu Y, Yang B, He Q and Dong X (2019) Phenotypic Screening-Based Identification of 3,4-Disubstituted Piperidine Derivatives as Macrophage M2 Polarization Modulators: An Opportunity for Treating Multiple Sclerosis. *J Med Chem* **62**(7): 3268-3285.

Wirtz E, Leal S, Ochatt C and Cross GA (1999) A tightly regulated inducible expression system for conditional gene knock-outs and dominant-negative genetics in Trypanosoma brucei. *Mol Biochem Parasitol* **99**(1): 89-101.

Wold MS (1997) Replication protein A: a heterotrimeric, single-stranded DNA-binding protein required for eukaryotic DNA metabolism. *Annu Rev Biochem* **66**: 61-92.

Woodring JL, Behera R, Sharma A, Wiedeman J, Patel G, Singh B, Guyett P, Amata E, Erath J, Roncal N, Penn E, Leed SE, Rodriguez A, Sciotti RJ, Mensa-Wilmot K and Pollastri MP (2018) Series of Alkynyl-Substituted Thienopyrimidines as Inhibitors of Protozoan Parasite Proliferation. *ACS Med Chem Lett* **9**(10): 996-1001.

Zhang Z, Barros-Alvarez X, Gillespie JR, Ranade RM, Huang W, Shibata S, Molasky NMR, Faghih O, Mushtaq A, Choy RKM, de Hostos E, Hol WGJ, Verlinde C, Buckner FS and Fan E (2020) Structure-guided discovery of selective methionyl-tRNA synthetase inhibitors with potent activity against Trypanosoma brucei. *RSC Med Chem* **11**(8): 885-895.

FOOTNOTES

**FIG. LEGENDS**

**Fig. 1. Delayed Cidal Concentration of CBL0137.** *T. brucei* ($1 \times 10^5$ cells/ml) was incubated with different concentrations of CBL0137 or DMSO (0.1%) for 6 h. Cell density was obtained with a Coulter Counter. Cells were rinsed and transferred to fresh drug-free HMI-9 medium at a density of $1 \times 10^4$ cells/ml and cultured at 37˚C for 48 h. Trypanosomes were enumerated in Coulter Counter or hemocytometer after 48 h. Curves were fit to data points using a non-linear function [ log (inhibitor) vs response – variable slope for four parameters] in Prism 9.0 (Graphpad). Bars indicate mean and SD.

**Fig. 2. Affinity chromatography and identification of CBL0137-binding proteins**

**Fig. 3. Nuclear DNA Synthesis is Inhibited by CBL0137.**

***Panel A,*** Scheme of the experimental protocol, and representative images for trypanosomes treated as described in the *Methods* section. For each condition, differential interference contrast microscopy (DIC), DAPI channel (blue), EdU channel (green), and merge between DAPI and EdU are presented. Images were captured using a DeltaVision II Olympus inverted microscope, and data were processed using Fiji (ImageJ, v 2.0.0). Data for integrated intensity was processed using CellProfiler 3.1.9 (Soliman, 2015). ***Panel B***, Analysis of rescaled integrated EdU fluorescence intensity in nuclei, drawn from three biological replicates. Bars indicate median and interquartile range. Kolmogorov-Smirnov test was used to assess statistical significance of differences in distribution of fluorescence intensity between DMSO and CBL01370137 treatment groups at $DCC_{25}$ ($p = 2.2 \times 10^{-6}$), $DCC_{50}$ ($p = 4.0 \times 10^{-6}$), and $DCC_{90}$ ($p < 1 \times 10^{-15}$). ***Panel C***, Analysis of the rescaled integrated intensity in the kinetoplast. Bars indicate median and interquartile range. Kolmogorov-Smirnov test was used to assess statistical significance of differences in fluorescence intensity between DMSO and CBL0137 treatment groups (Soliman, 2015).

**Fig. 4. CBL0137 Inhibits Mitosis.** *Trypanosoma brucei* Lister 427 (5 x $10^5$ cells/ml) in HMI-9 medium were exposed to DMSO (0.1 %), or CBL0137 (180 nM) at 37˚C, 5% $CO_2$ for 6 h. Trypanosomes were harvested and fixed in paraformaldehyde (4%) in PBS, applied to pre-coated coverslips with 0.01 % of polylysine in PBS, and mounted in Vectashield with DAPI (5 µM). Cells were visualized using an EVOS-FL microscope (Thermofisher), and numbers of kinetoplasts and nuclei counted. *Panel A,* Experimental strategy. *Panel B,* Cell type quantitation after treatment of trypanosomes with CBL0137 (different amounts) or DMSO (vehicle for CBL0137). K = kinetoplast; N = nucleus. *Panel C,* Images (brightfield or DAPI-stained nuclei or kinetoplasts) of trypanosomes after treatment with CBL0137 (180 nM) or DMSO (solvent control). Horizontal lines represent means. Statistical significance of differences in distributions of cell types was analyzed with a Chi-square test ($p = 1 \times 10^{-7}$) using Prism 9.0 (Graphpad).

**Fig. 5. RPA1 knockdown inhibits DNA replication and blocks mitosis.** RNAi against RPA1 was induced for 18 h with tetracycline (1 µg/ml). *Panel A,* Representative images for non-induced and induced RPA1 knockdown cells. DIC (first column), DAPI (blue channel), nuclear fluorescence of V5-RPA1 (green channel). Control antibody YL1/2 (recognizes basal bodies) (magenta channel). *Panel B* and *Panel C* Analysis of the fluorescence intensity of RPA1 and basal-body signals for cells induced or un-induced with tetracycline. Bars represent median and interquartile range. Kolmogorov-Smirnov test was used to assess statistical significance of differences in distribution of fluorescence data between – and + tetracycline treatment ($p = 4.1 \times 10^{-5}$, and p = 0.2996 for panel B and C, respectively). *Panel D*, Representative images of EdU assays for non-induced and induced cells; DIC, DAPI (blue channel), EdU (green channel), and merge of DAPI and EdU. *Panel E*, Quantitation of the percentage of EdU-positive cells from three biological replicates. Statistical significance of differences in means was determined with a paired Student t-test ($p = 1.8 \times 10^{-3}$). *Panel F*, Intensity of fluorescence of nuclear EdU in

induced or uninduced cells. Statistical significance of differences of distributions of data points from the two conditions was calculated with a Kolmogorov-Smirnov test ($p < 1 \times 10^{-15}$). **Panel G**, Distribution of trypanosome types after 18 h of inducing knockdown of RPA1. Possible statistical significance of differences in distributions was calculated with a chi-square ($X^2$) test; $p = 2.84 \times 10^{-35}$. All statistical analysis was performed using Prism 9.0 (Graphpad). Horizontal lines represent means.

**Fig. 6. RPA2 Knockdown Inhibits Mitosis and Produces Anucleate Trypanosomes.**

Trypanosomes expressing a c-terminus Myc-tagged RPA2 were transfected with an RNAi construct targeting RPA2. Stable transfectant clones were induced with tetracycline (1 µg/ml) for different the times indicated. **Panel A,** Western blot using $3 \times 10^6$ cells/lane of control (single-marker (SM) trypanosomes) and RPA2-Myc RNAi cell line. Primary antibody Anti-Myc (9E10) rabbit mAb (Santa Cruz Biotech) was diluted 1:2500 in Intercept-PBS blocking solution (LI-COR) plus 0.2 % of Tween-20. Secondary antibody was IRDye-800 anti-mouse (LI-COR) diluted 1:20000 (in Intercept-PBS, 0.2 % of Tween-20, and 0.2% of SDS). **Panel B,** Quantitation of magnitude of change in RPA2-Myc between induced and uninduced trypanosomes from three biological replicates. A paired Student t-test was used to determine statistical significance of differences in mean values ($p = 0.012$). **Panel C**, Trypanosome proliferation-time course for RPA2 knockdown and controls. Three biological replicates were studied, each with trypanosomes at a starting density of $1 \times 10^5$ cells/ml. Cultures were 10-fold to continue the study when density reached $1 \times 10^6$ trypanosomes/ml. **Panel D,** Distribution of different trypanosome types after 24-h knockdown of RPA2. A Chi-square test using Prism 9.0 (Graphpad) was used to determine the possible statistical significance of differences in the distribution of cell types ($p = 4.87 \times 10^{-29}$). Horizontal lines represent means. Two RNAi cell lines for RPA2 were studied; they produced similar results.

**Fig. 7. UMSBP2 Knockdown Does Not Affect DNA Replication or Nucleus Mitosis.**

Trypanosomes stably expressing a V5-tagged (at n-terminus) UMSBP2 were transfected with a

UMSBP2 RNAi construct, and clonal lines selected *(Materials and Methods).* RNAi was induced

with tetracycline 1 µg/ml. **Panel A**, Western-blot using 3 x $10^6$ cells/lane of control (SM

trypanosomes) or UMSBP2-RNAi trypanosome line induced for 24 h. The primary antibody was

anti-V5 (D3H8Q) rabbit mAb (Cell Signaling Technology) diluted 1:3000 (in Intercept-PBS

blocking solution (Li-COR) plus 0.2 % of tween-20). Secondary antibody was IRDye-800 anti

Rabbit (Li-COR) diluted 1:20000 (in Intercept-PBS, 0.2 % of Tween-20, and 0.2% of SDS).

**Panel B**, Quantitation of changes in V5-RPA1 protein level between induced and uninduced

cells from three biological replicates. A paired student t-test was used to determine the possible

statistical significance ($p$ = 0.002) of differences in mean values. **Panel C**, Proliferation versus

time curves for UMSBP2 knockdown or control trypanosomes. Cell were seeded at 1 x $10^5$

cells/ml, and cell density was determined with a Coulter-Counter. Cultures reaching a density of

1 x $10^6$ cells/ml, were diluted 10-fold to continue the experiment. Three biological replicates

were obtained for each trypanosome line.  **Panel D**, Distribution of different cell types after 24 h

of induction. A Chi-square test was used to calculate the possible significance of the differences

in distribution of cell types *($p$ = 0.1514)*. Two RNAi clonal lines for UMSBP2 were studied, and

they produced very similar results. All statistical analysis was performed using Prism 9.0

(Graphpad)

**Fig. 8. CBL0137 alters proteostasis in the trypanosome.** Clonal lines of *T. brucei* stably

transfected with epitope-tagged forms of one of three proteins, namely V5-RPA1, V5-

Tb427.tmp160.4770, Tb427.03.1010-V5 were selected. **Panel A**, scheme of experimental

procedure. Trypanosomes were inoculated at 1 x $10^5$ cells/ml and incubated with or without

DMSO, or CBL0137 (725 nM) for 6 h. Cell lysates were electrophoresed and transferred to a

PVDF membrane (Bio-Rad). Each lane (for electrophoresis) was loaded with 1 x $10^6$ cell

equivalents of lysate, except V5-RPA1 where $3 \times 10^6$ equivalents of lysate was used. Primary antibody was anti-V5 (D3H8Q) rabbit mAb (Cell Signaling) diluted 1:3000 in Tris Base Saline Buffer (20 mM Tris, 150 mM NaCl) with 0.1% of Tween 20 at pH 8.0 (TBST). Secondary anti-rabbit antibody coupled to alkaline phosphatase (Bio-Rad) was diluted 1:3000 in TBST and incubated with the membrane for 1 h, after which the membrane was developed with an alkaline phosphatase reagent (Bio-Rad). The experiment was performed three times with different biological samples. *Panel B* (Upper panel), a representative western blot for each tagged protein is presented with the arrow pointing to the anti-V5 signal. *Panel C*   Loading control image of a Stain-Free gel detected using ChemiDoc XRS+ (Bio-Rad) *Panel D*, Normalized quantitation for three biological replicates of each experiment. For normalization the anti-V5 signal was corrected for total protein in the entire lane.  A paired student t-test was used to determine statistical significance in means of the data from the three biological replicates ($p$-value between DMSO control and treated samples were $2.3 \times 10^{-3}$, $2.4 \times 10^{-3}$ and $2 \times 10^{-3}$, for V5-RPA1, V5-NRP1 and Tb427.03.1010-V5, respectively). Statistical analysis was performed using Prism 9.0 (Graphpad). Horizontal lines represent means.

**Fig. 9. CBL0137 inhibits protein synthesis.**

*Panel A*, Scheme of the experimental protocol. *T. brucei* ($5 \times 10^5$ cell/ml) was incubated with DMSO (0.1%) or different concentrations of CBL0137 for 15 min before HPG addition, and "click-chemistry" with Azide-PEG3-biotin. Cycloheximide was added at $DCC_{90}$ concentration (85 µM) as a positive control. *Panel B,* A representative western-blot ($1 \times 10^6$ cell equivalents of lysate per lane) probed with IRDye-streptavidin 800 CW (1:2500 dilution) (LI-COR). Total protein was tracked using REVERT protein stain (Li-COR). Images were captured using Odyssey CLx (LI-COR), and data processed using Image Studio Lite Quantitation Software v 5.2.5 (LI-COR). *Panel C*, Quantitation of CBL0137 effects on nascent polypeptide synthesis. Total protein from each lane (lane 7-to-lane 12) was used as a correction factor for HPG

incorporation in each lane (lanes 2-lane 6) (*i.e.*, normalized streptavidin fluorescence). Three

biological replicates were tested. A paired two-sided student t-test (Prism 9.0, GraphPad) was

used to compare differences in means of normalized fluorescence intensities between DMSO

(control) and CHX or CBL0137-treated trypanosomes. Horizontal lines denote means.

**Fig. 10. Summary of Molecular Modes of CBL0137 Action**

***Panel A***. Molecular effects of CBL0137 on three pathways are listed below the arrows, with +

indicating inhibitory effect, and – for no effect. At $DCC_{25}$ CBL0137 inhibits DNA replication and

mitosis, and at $DCC_{50}$ the drug also blocks protein synthesis. ***Panel B***. Effect of knockdown of

CBL0137-binding proteins on mitosis, DNA replication, polypeptide translation, and emergence

of XK1N (multi-kinetoplasts, one nucleus) or 1K0N (anucleate) trypanosomes.

**TABLES**

**Table 1. Proteins that bind a curaxin-affinity column.** Proteins in a trypanosome lysate were adsorbed to agarose-Curaxin beads (see *Materials and Methods*). After washing with phosphate buffered saline (PBS), proteins bound to the affinity column were eluted with buffer containing CBL0137 (50 μM), and identified by mass spectrometry (*Materials and Methods*). Table presents proteins identified after mass spectrometry of eluates from the curaxin-affinity column. A posterior Error Probability value (PEP-value; the probability that the peptide spectrum match (PSM) is incorrect (Kall et al., 2008; Kall et al., 2009) was calculated in Proteome Discoverer (Orsburn, 2021; Palomba et al., 2021).

**Table 1**

| Gene ID | Description | Peptide sequences Identified in TritrypDB | N of times peptide was identified | PEP-value | Spectral Counts | |
|---|---|---|---|---|---|---|
| | | | | | Azide Agarose Bead (Control) | Curaxin Affinity beads |
| | | | | | Average | Average |
| **Metabolic Enzymes** | | | | | | |
| Tb427.10.5620 | Fructose-bisphosphate aldolase | TDCGLEPLVEGAK | 3 | $1.67 \times 10^{-3}$ | 15.7 ± 4.0 | 34.3 ± 7.5 |
| Tb427.06.4280 | Glyceraldehyde-3-phosphate dehydrogenase | NPADLPWGK | 2 | $1.82 \times 10^{-2}$ | 7.0 ± 4.0 | 16.0 ± 1.7 |
| Tb427.03.3270 | ATP-dependent phosphofructokinase | TIDNDLSFSHR | 3 | $2.3 \times 10^{-3}$ | 5.7 ± 2.1 | 15.3 ± 1.5 |
| Tb427.01.700 | Phosphoglycerate kinase | VDFNVPVK | 2 | $5.7 \times 10^{-2}$ | | 4.0 ± 1.0 |
| Tb427.08.6390 | lysophospholipase | FLQQVLPGPSSK | 1 | $4.3 \times 10^{-3}$ | | 3.5 ± 2.1 |
| Tb427.10.16120 | Inosine-5'-monophosphate dehydrogenase | GISGILVTEGGK | 1 | $1.95 \times 10^{-2}$ | | 3.5 ± 2.1 |
| **DNA Associated proteins** | | | | | | |
| Tb427.10.6060 | Universal minicircle sequence binding protein2 | ACYHCQQEGHIAR | 3 | $2.4 \times 10^{-4}$ | | 11.7 ± 8.7 |
| Tb427.05.1700 | Replication protein A 28 kDa subunit (RPA2) | ITDGTGVVVVR | 3 | $2.6 \times 10^{-3}$ | | 4.3 ± 3.2 |
| Tb427tmp.01.0870 | Replication protein A1 (RPA1) | VKEEGLGGNEDSER | 2 | $3.3 \times 10^{-4}$ | | 3.3 ± 3.2 |
| **RNA Associated proteins** | | | | | | |
| Tb427tmp.211.2150 | Poly(A)-binding protein 2 (PABP 2) | NFDDTVTSER | 3 | $6.6 \times 10^{-3}$ | | 11.7 ± 3.5 |
| Tb427.04.2040 | ALBA-Domain Protein | SAVGVAEVLK | 3 | $2.4 \times 10^{-3}$ | | 7.3 ± 1.5 |
| Tb427tmp.211.4540 | RNA-binding protein DRBD2 | ETFQQVGEVER | 2 | $2.9 \times 10^{-2}$ | | 4.7 ± 2.5 |
| Tb427tmp.211.0560 | RNA-binding protein DRBD3 | NNEIGEVSR | 2 | $5.3 \times 10^{-3}$ | | 3.5 ± 3.5 |
| Tb427tmp.160.3270 | Eukaryotic Initiation Factor 4A-1 | GGDIIAQAQSGTGK | 2 | $1.9 \times 10^{-3}$ | 2.0 | 2.5 ± 0.7 |

**Figure 1.**

**Figure 2.**

Azide agarose beads

"Curaxin Class 3 Affinity Tag"

$1 \times 10^8$ cells

Lysate

Copper catalyzed "Click" reaction

Curaxin Class 3 affinity beads

Chromatography in agarose-CBL0137. Elute with CBL0137 (50 µM)

Identify peptides in MS

m/z
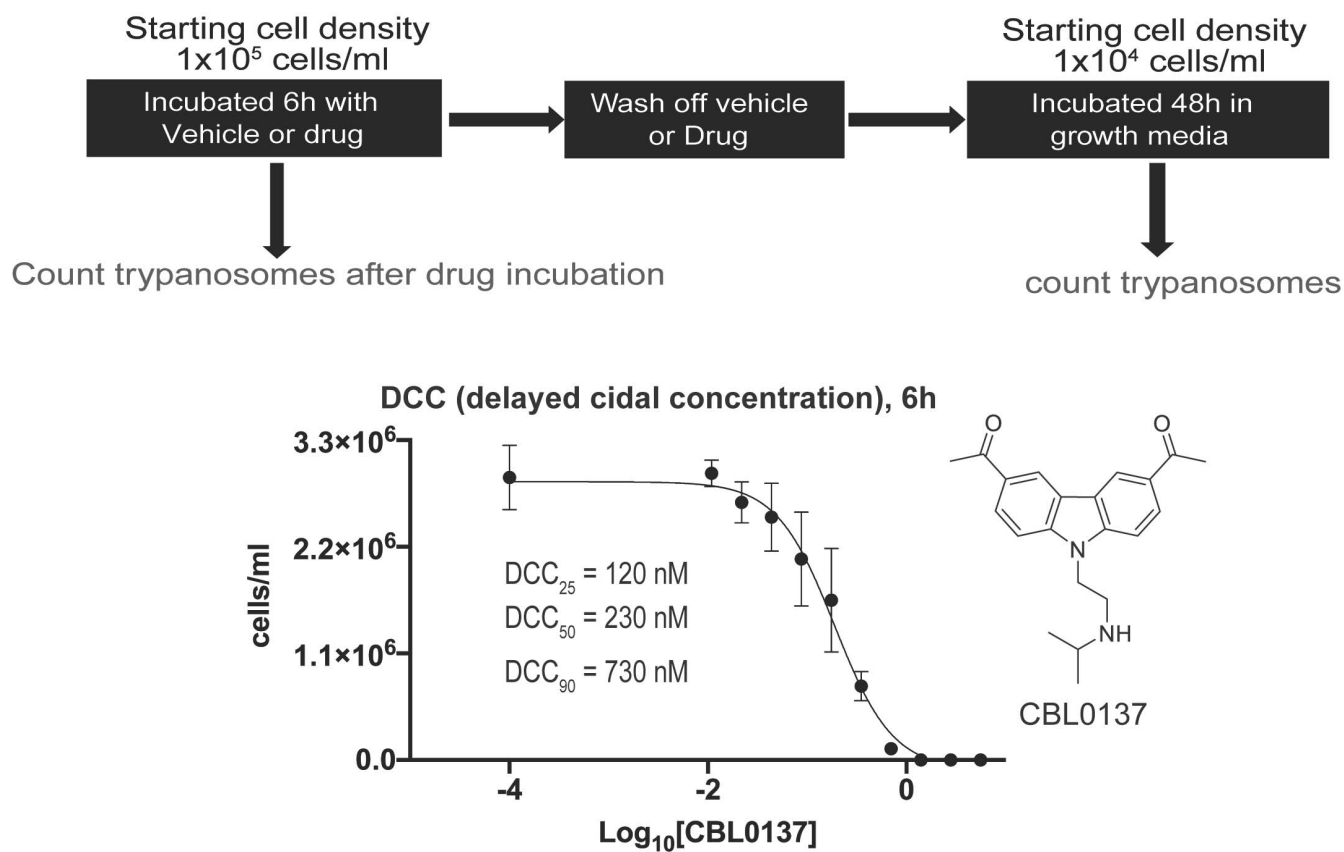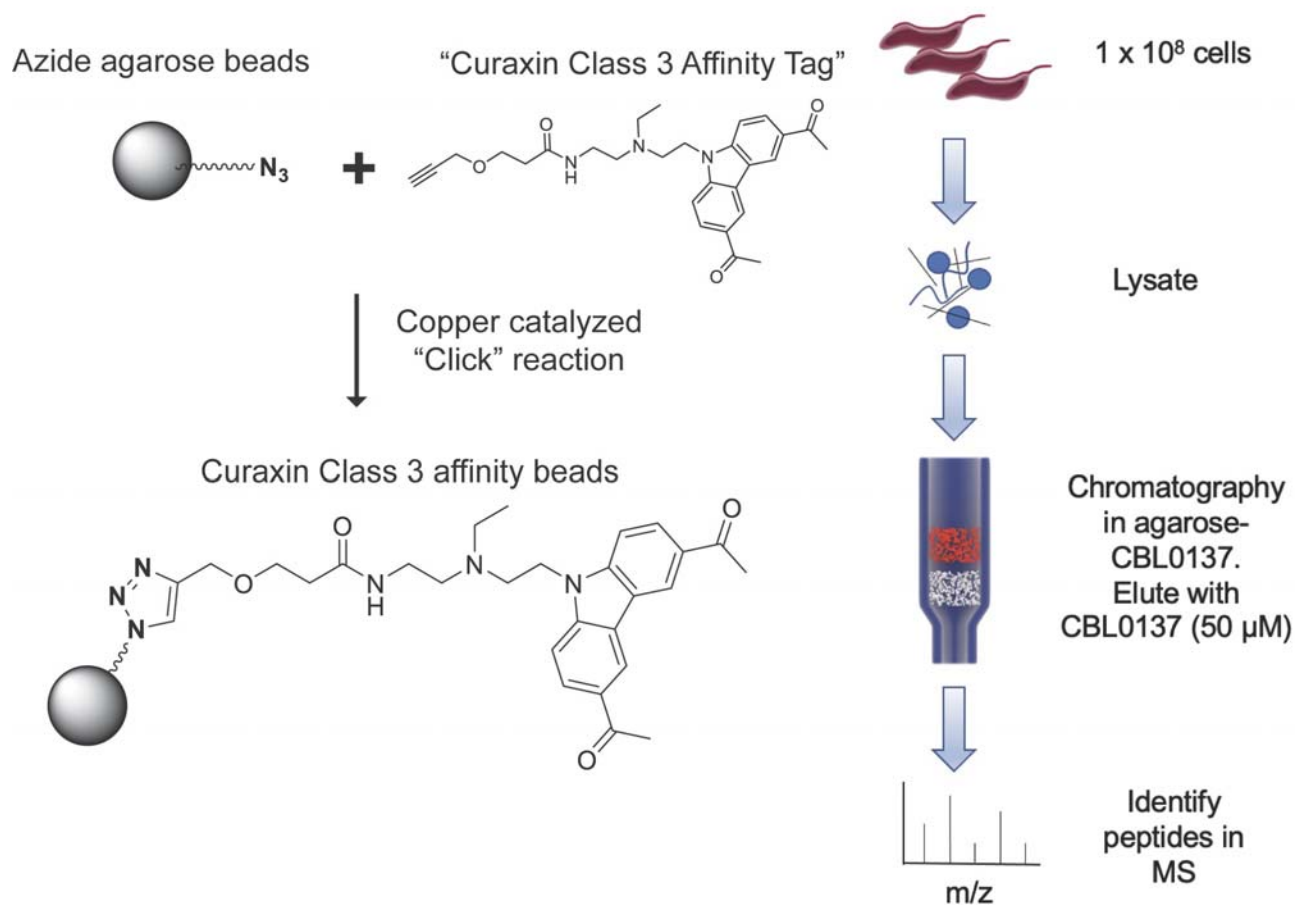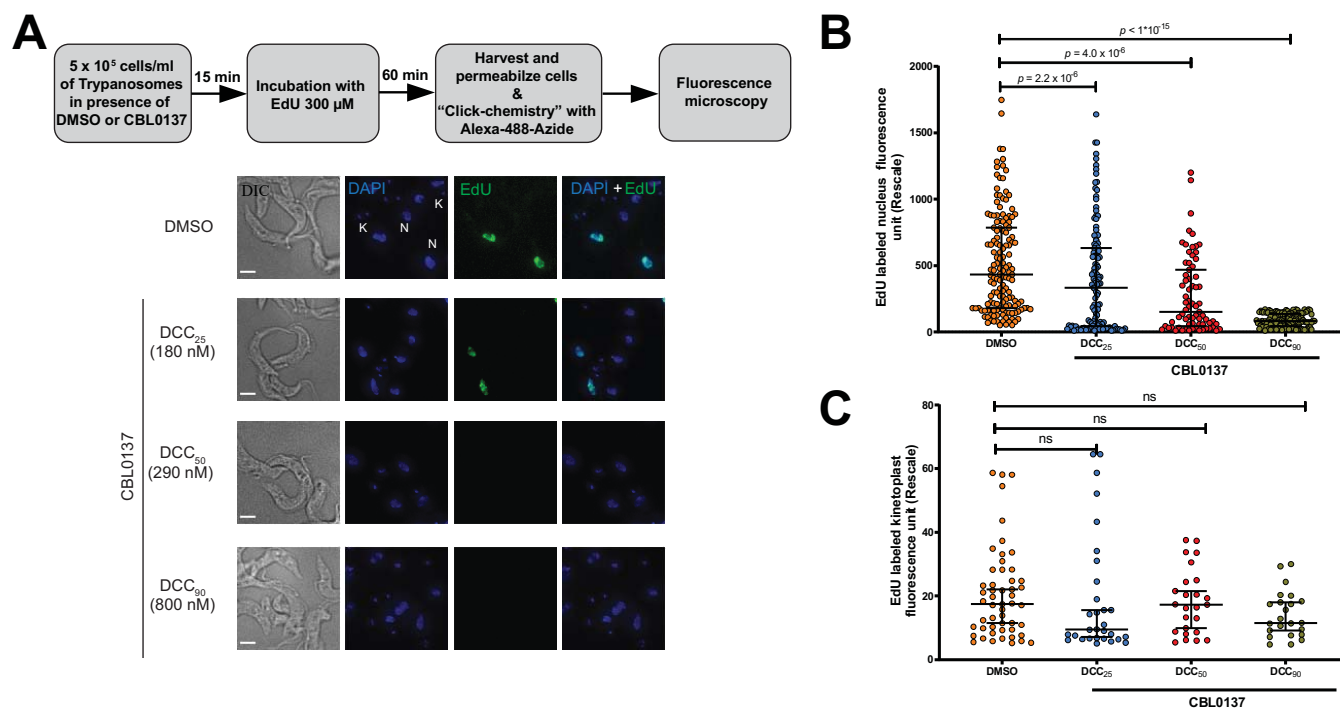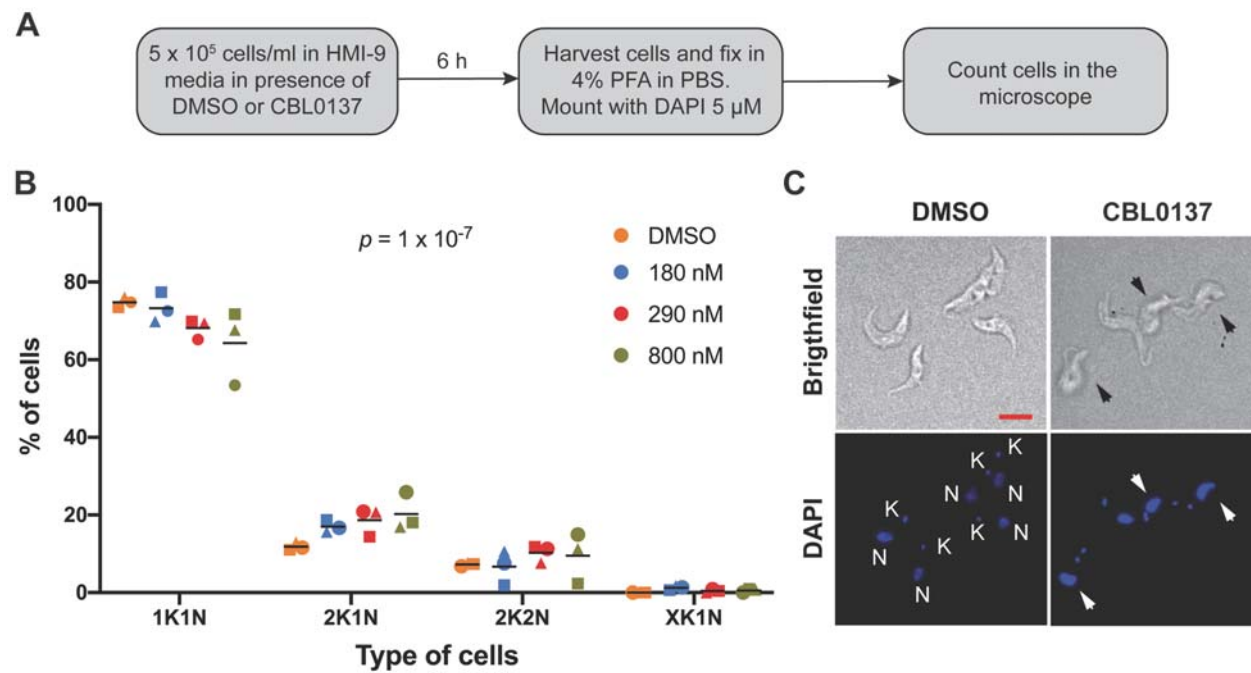
# Figure 3.

**Figure 4.**

**Figure 5.**
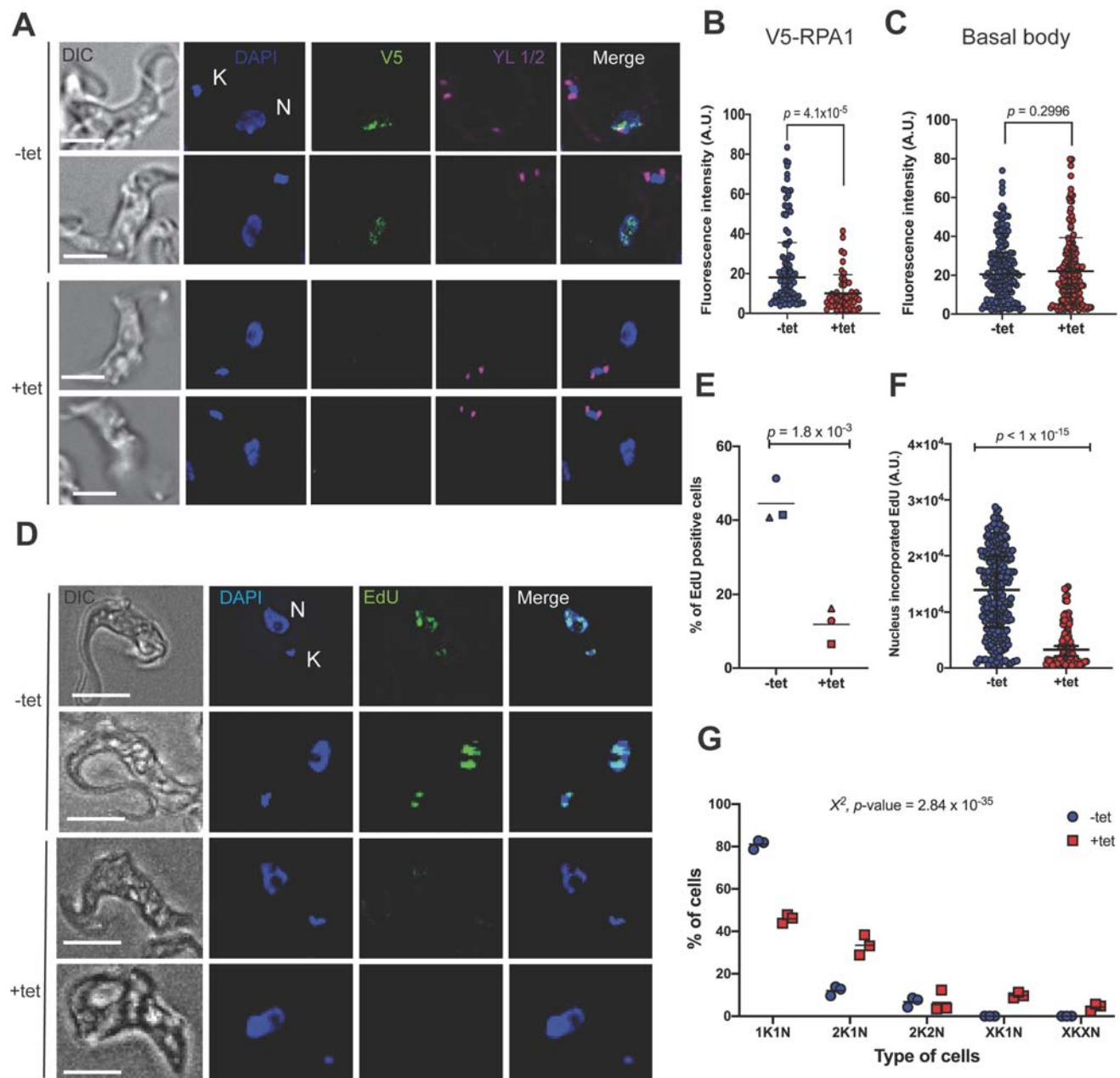
**Figure 6.**

**Figure 7.**

# Figure 8.

**A**



| *T. brucei* tagged cell line $1 \times 10^5$ cells/ml. | → | Incubated with DMSO or CBL0137 at $DCC_{90}$ | —6 h→ | Harvest cells, resuspend in Sample Buffer and perform western blot using V5 anti-body. |

**B**



**C**

**D**
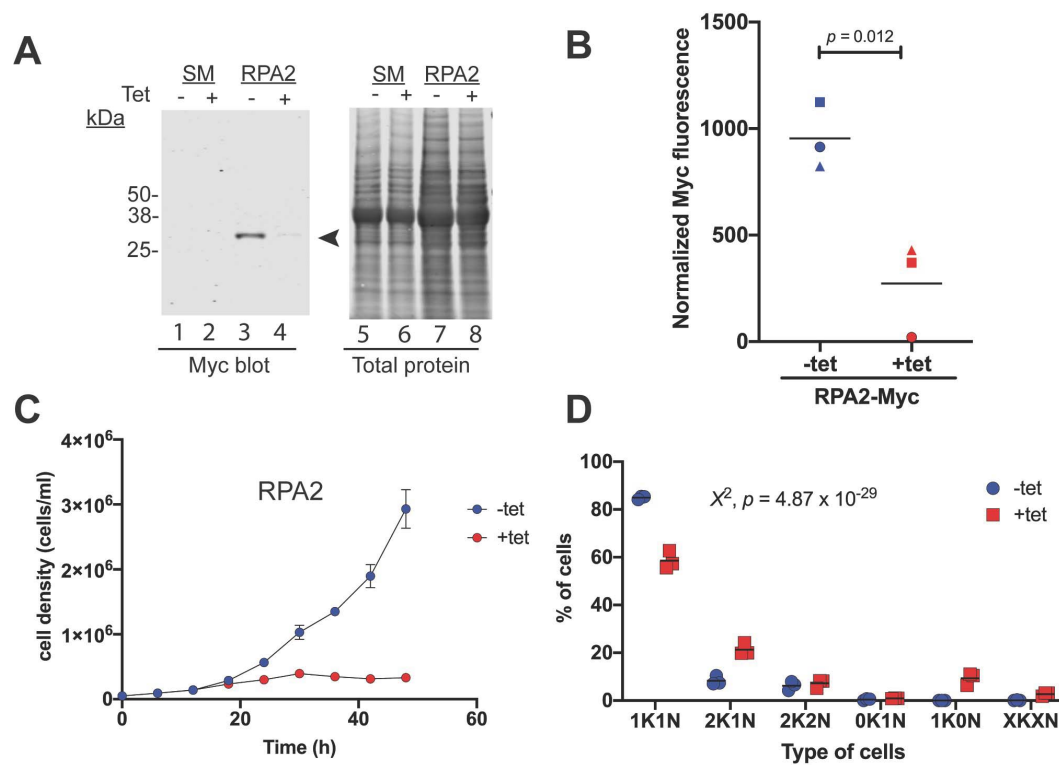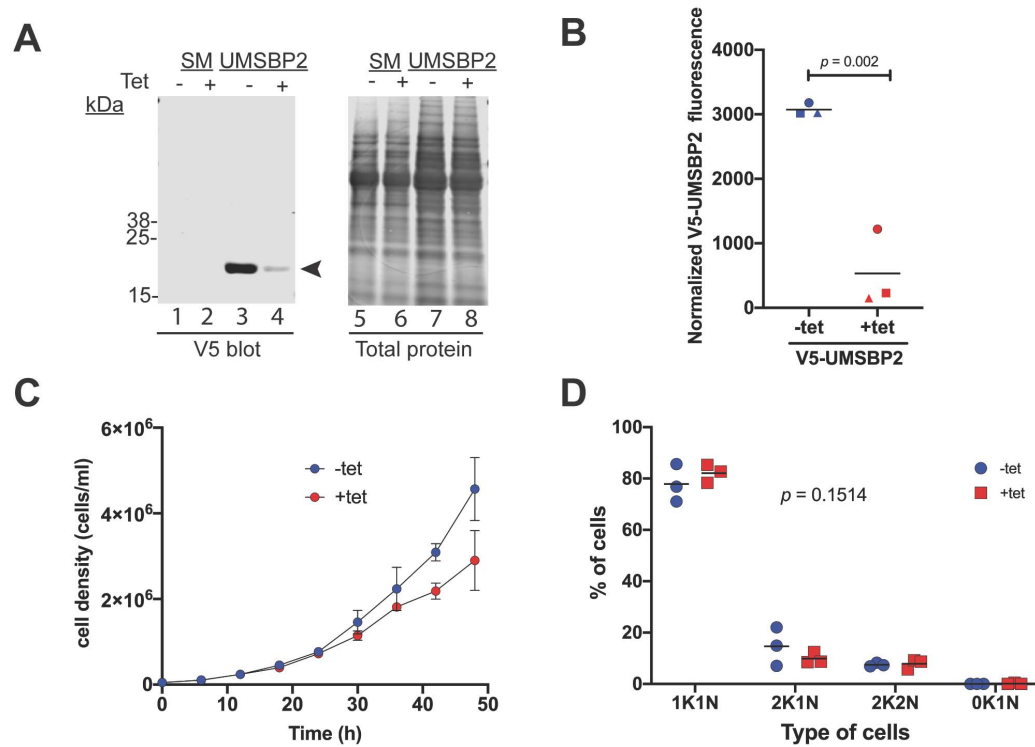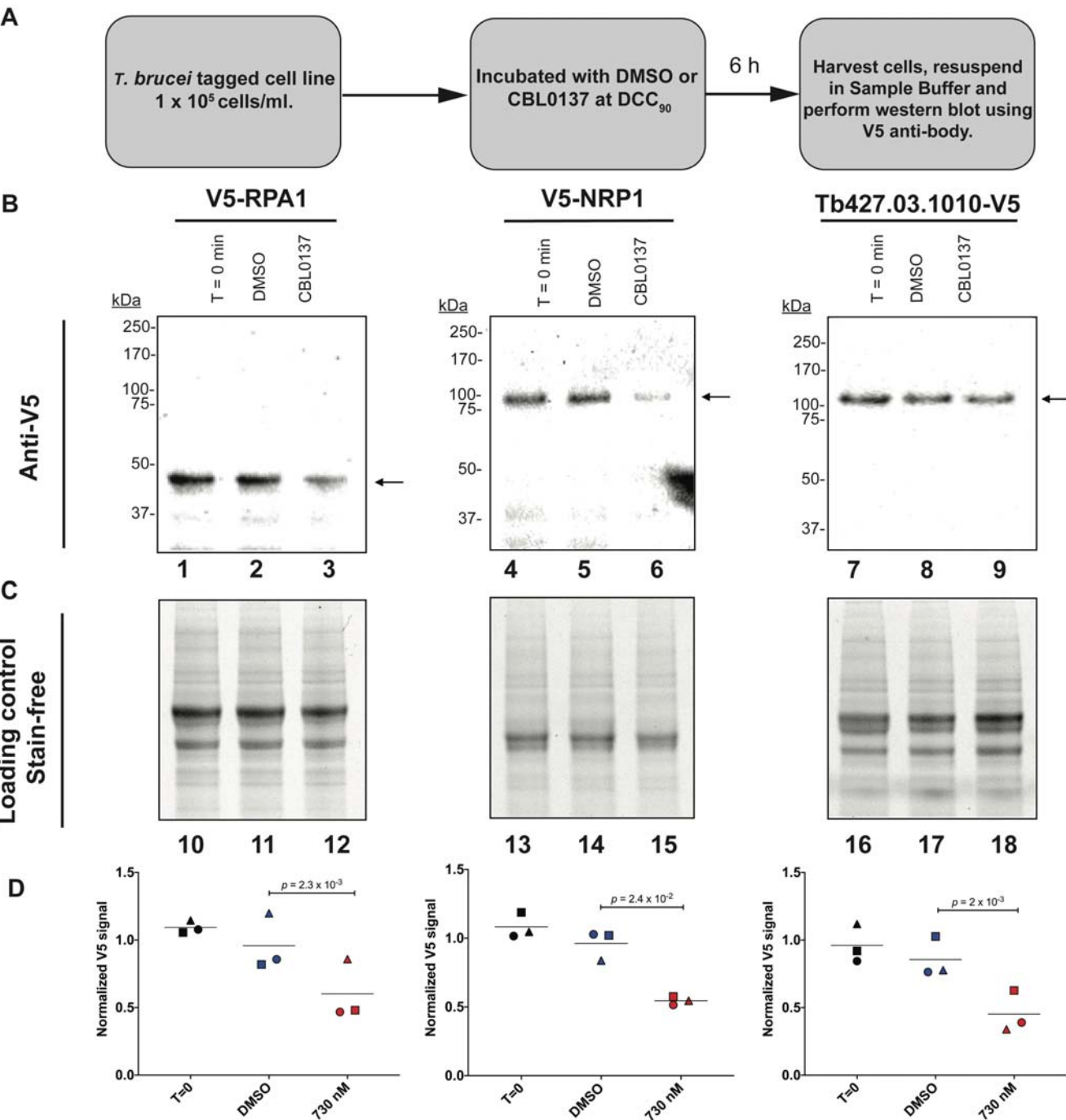
**Figure 9.**

**Figure 10.**

**A**
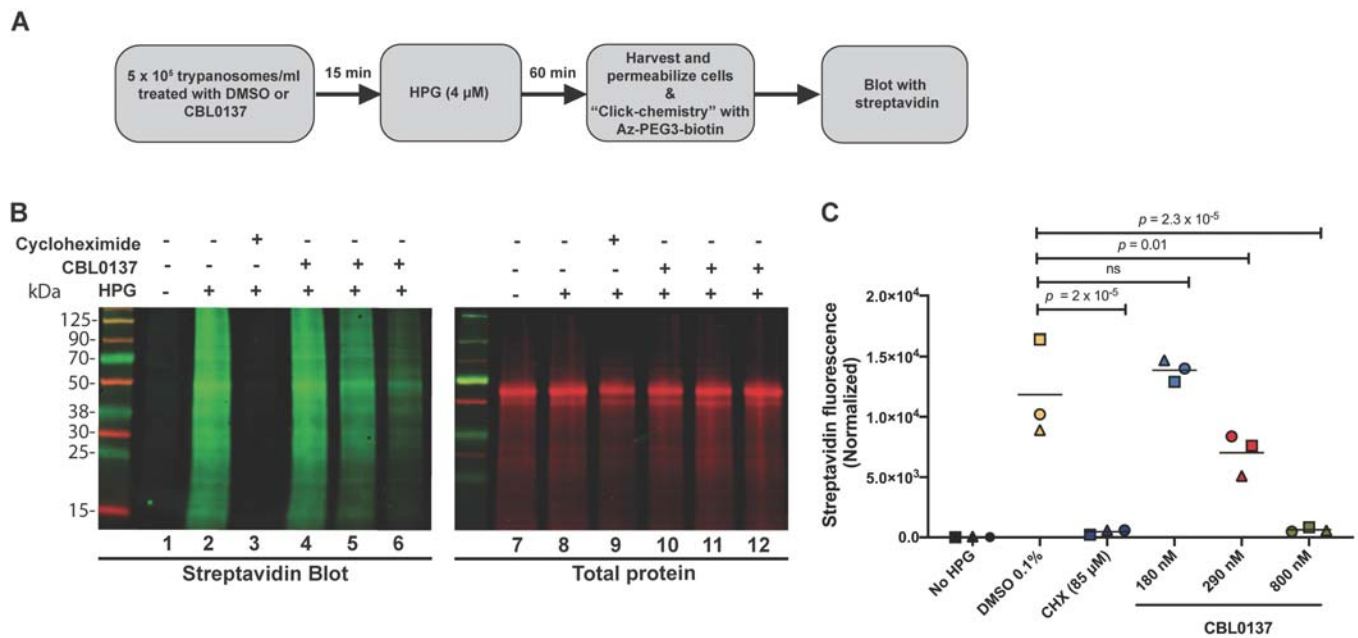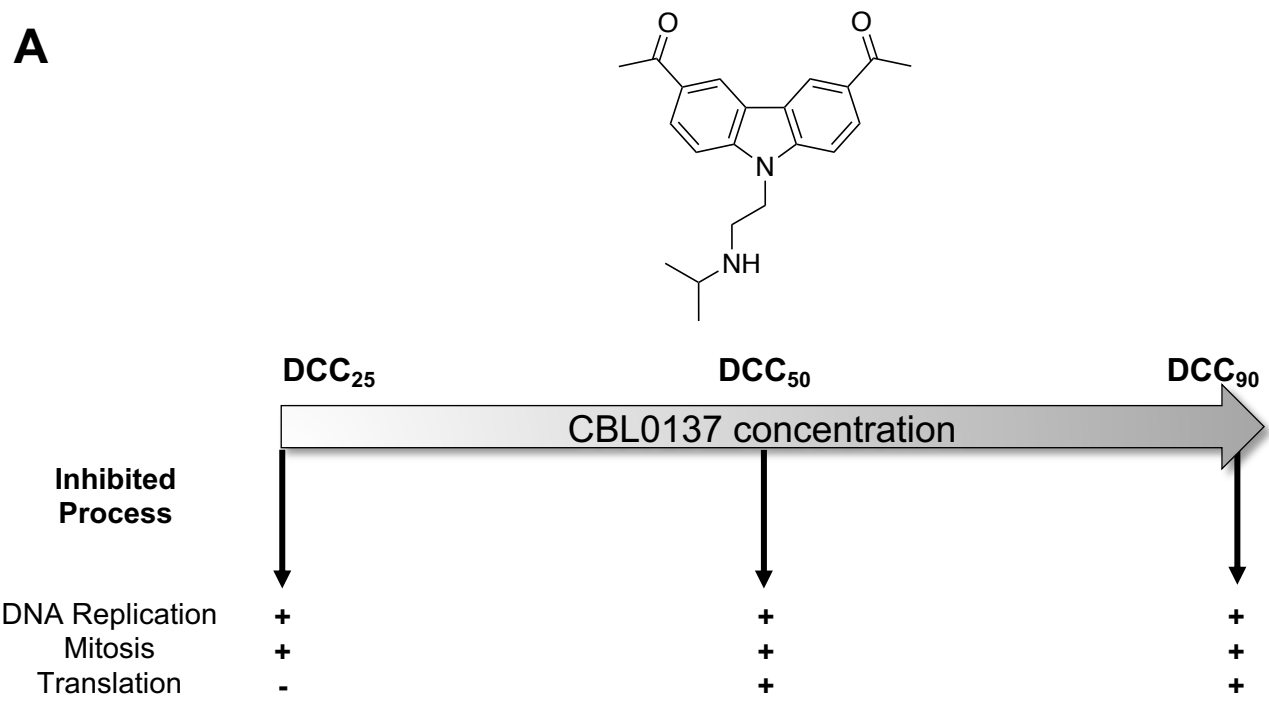


| Gene | Mitosis inhibition | DNA replication inhibition | Translation inhibition | XK1N present | 1K0N present |
|------|--------------------|----------------------------|------------------------|--------------|--------------|
| RPA1 | yes | yes | no | yes | no |
| RPA2 | yes | ND | ND | no | yes |
| UMSBP2 | no | ND | ND | no | no |

**B**

MOLPHARM-AR-2021-000430R2

**Physiologic Targets and Modes of Action for CBL0137, a Lead for Human African Trypanosomiasis Drug Development**

*Carlos E. Sanz-Rodríguez[2], Benjamin Hoffman[2], Paul J. Guyett[2], Andrei Purmal[3], Baljinder Singh[4], Michael Pollastri[4], and Kojo Mensa-Wilmot[1,2]\**

**Generation of RNAi construct.**

Primers for each RNAi construct were generated using RNAit2 software with *Trypanosoma brucei* 427 genome as a reference (Redmond, 2003). Digestion sites for BamH I and Xho I were added in the forward and reverse primers, respectively. For primer amplification, genomic DNA from *T. brucei* 427 bloodstream was used as a template. Digested inserts were cloned into p2T7[TABlue] trypanosome RNAi vector (Alibu et al., 2005). Digested insert-p2T7[TABlue] constructs were linearized using NotI-HF (NEB, Ipswich, MA), and transfected into *T. brucei* bloodstream Single Marked (SM) by nucleofection (Guyett et al., 2016; Subramanya and Mensa-Wilmot, 2006; Wirtz et al., 1999). For each of the proteins under the study, the SM line used was tagged with V5 or Myc tag. Following transfection, trypanosomes were diluted in 40 ml of HMI-9 and incubated for 24 h. Then, the culture was diluted serially (1:10, 1:100, 1:1000) and each dilution plated (1 ml/well) in a 24-well plate. Stable transfectant clones were selected in the presence of G418 (6.5 µg/ml), hygromycin B (5 µg/ml), and blasticidin (5 µg/ml) for V5 tag cell lines or puromycin (0.1 µg/ml) for Myc tag cell line. The primers used for the RNAi construct are shown in Table S2.

**V5 and Myc tag cell lines.**

A blasticidin (bla)/V5 plasmid (provided by Dr. Christian Tschudi, Yale University) was used as a template to amplify a bla/V5 tagging cassette flanked by sequences specific to Tb-V5-UMSBP2 or V5-RPA1. For RPA2-Myc a Myc/puromycin plasmid (provided by D. Roberto Docampo, University of Georgia) was used as a template to amplify a Myc tagging /puromycin cassette

flanked by sequence specific to RPA2. A V5/blasticidin plasmid (Genewiz) was used as a

template to amplify a V5 tagging/blasticidin cassette flanked by sequence specific to CK1.2 and

Tb427.03.1010-V5. For CK1.2 HA/hygromycin B and pMoTag4H was used with primers used

for tagging (Table S3).

**ATP synthesis assay.**

*Extract preparation:* Trypanosomes ($5 \times 10^5$ /ml) were incubated at 37˚C in DMSO (negative

control), or CBL0137 at 180, 290 and 800 nM ($DCC_{25}$, $DCC_{50}$, $DCC_{90}$, respectively). As poaitive

control, 2-Deoxyglucose (2mM), and $NaN_3$ (3 mM) were used. After 1 h, $6 \times 10^5$ cells/ml were

washed in cold PBS, were resuspended in 150 µl of cold deionized $H_2O$ and incubated on ice

for 10 min. Then, 150 µl of cold PBS 2X was added, and cells were quick frozen in liquid $N_2$ and

thawed on ice.

 *ATP measurement by bioluminescence*: Trypanosome lysate (from above) (100 µl ) was mixed

with 100 µl of ATP assay mix (Adenosine 5` triphosphate (ATP) Bioluminescence Assay Kit,

Sigma-Aldrich, Cat number FLAA) on ice and added to a well in a white 96-well plate, followed

by 3 min of slow shaking on a rotator. Luminescence was read using Varioskan™ LUX

multimode plate reader (Thermo Fisher). An ATP calibration curve was constructed.  Two

technical replicates per sample obtained and three biological replicates were studied for each

measurement.
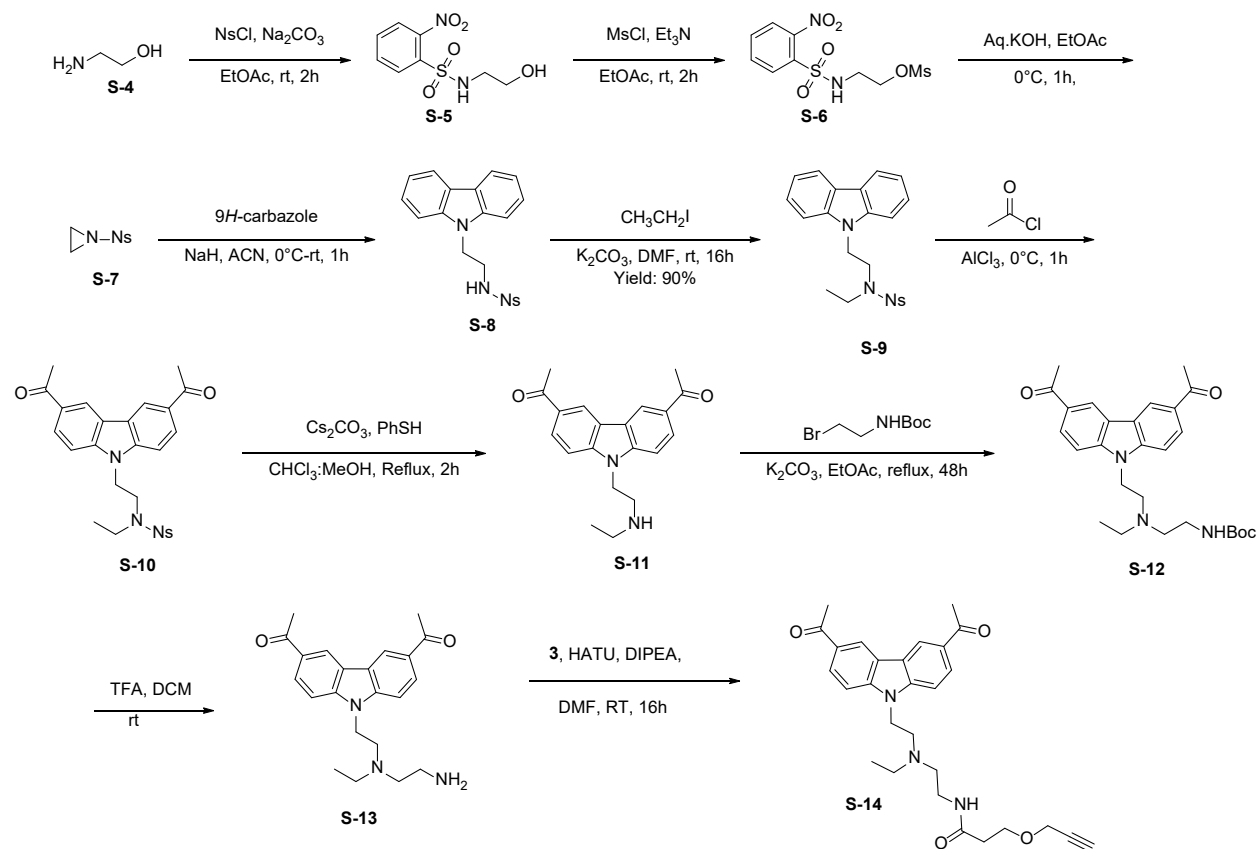
**Synthesis of alkyne derivative of Curaxin Class 3**
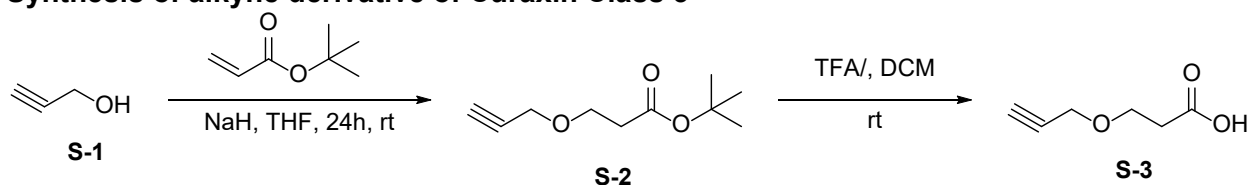


**Scheme 1:** Synthesis of alkyne tag

**Synthesis of tert-butyl 3-(prop-2-yn-1-yloxy)propanoate (S-2).** To an ice-cold solution of prop-2-yn-1-ol **S-1** (1.0 g, 17.84 mmol) in THF (20 mL) was added sodium hydride (60% dispersion in mineral oil, 0.1 g, 2.67 mmol) portion-wise. The reaction mixture was stirred at 0°C for 10 min, followed by addition of tert-butyl acrylate (1.59 g, 12.48 mmol). The resulting reaction mass was stirred at room temperature for 24 h. After the completion of the reaction, the reaction mass was diluted with water (100 mL) and extracted with EtOAc (3 x 100 mL). The combined organics were washed with $H_2O$ (3 times) and brine respectively. The organic fraction was dried over anhydrous $Na_2SO_4$, filtered and concentrated under reduced pressure to get desired product **3** as colorless liquid (1.3 g, yield: 40%). $^1$H NMR (400 MHz, CDCl$_3$) δ 4.15 (s, 2H), 3.74-3.77 (m, 2H), 2.49-2.52 (m, 2H), 2.42 (s, 1H) and 1.44 (s, 9H). LCMS found 185.22 [M+H]$^+$.

**Synthesis of 3-(prop-2-yn-1-yloxy)propanoic acid (S-3).** An ice-cold solution of tert-butyl 3-(prop-2-yn-1-yloxy)propanoate **S-2** (1.3 g, 7.06 mmol) in TFA:DCM (1:1, 10 mL) was stirred at room temp. for 3h. After the completion of the reaction, the reaction mass was concentrated under reduced pressure to get desired product **S-3** as colorless liquid (0.9 g, yield: 99%). $^1$H NMR (400 MHz, DMSO-d$_6$) δ 12.22 (br s, 1H), 4.11 (s, 2H), 3.59-3.64 (m, 2H), 3.42 (s, 1H) and 2.44-2.47 (m, 2H). LCMS found 127.0 [M-H]$^+$.

MOLPHARM-AR-2021-000430R2



**Scheme 2:** Synthesis of alkyne derivative (**S-14**)

**Synthesis of *N*-(2-hydroxyethyl)-2-nitrobenzenesulfonamide (S-5).** To a solution of ethanolamine (3.22 mL, 53.61 mmol) in ethyl acetate (20 mL) was added solution of sodium carbonate (6.9 g, 65.80 mmol) in water (30 mL). The reaction mixture stirred at rt for 5-7 min followed by addition of a solution of 2-nitrobenzenesulfonyl chloride (10 g, 48.74 mmol) in ethyl acetate (30 mL). The resulting reaction mass was stirred at rt for 2 h. After the completion of the reaction, the reaction mass was diluted with water (100 mL) and extracted with EtOAc (3 x 100 mL). The combined organics were washed with $H_2O$ (3 times)**,** saturated solution of citric acid and brine respectively. The organic fraction was dried over anhydrous $Na_2SO_4$, filtered and concentrated under reduced pressure to get desired product **S-5** as off white solid (10 g, yield: 83%). $^1$H NMR (400 MHz, CDCl$_3$) δ 8.13-8.15 (m, 1H), 7.87-7.89 (m, 1H), 7.74-7.76 (m, 2H),

5.73 (br s, 1H), 3.73-3.77 (m, 2H), 3.24-3.28 (m, 2H) and 1.76-1.79 (br s, 1H). LCMS found

245.12 [M-H]$^+$.

**Synthesis of 2-((2-nitrophenyl)sulfonamido)ethyl methanesulfonate (S-6).** To an ice-cold

solution of *N*-(2-hydroxyethyl)-2-nitrobenzenesulfonamide **S-5** (10 g, 40.61 mmol) in ethyl

acetate (70 mL) was added triethylamine (6.8 mL, 48.73 mmol) and methanesulfonyl chloride

(3.5 mL, 44.67 mmol) in EtOAc (10 mL). The resulting reaction mass was stirred at rt for 2 h.

After the completion of the reaction, the reaction mass was filtered to remove the precipitates of

triethylamine hydrochloride. The filtrate was washed with aqueous NaHCO$_3$ and H$_2$O (3 times).

The organic fraction was dried over anhydrous Na$_2$SO$_4$, filtered and concentrated under

reduced pressure to get desired product **6** as off-white solid (10 g, yield: 77%). $^1$H-NMR (400

MHz, CDCl$_3$): δ 8.12-8.15 (m, 1H), 7.89-7.91 (m, 1H), 7.76-7.78 (m, 2H), 5.85 (br s, 1H), 4.28-

4.31 (m, 2H), 3.44-3.52 (m, 2H) and 3.02 (s, 3H). LCMS found 323.14 [M-H]$^+$.

**Synthesis of 1-((2-nitrophenyl)sulfonyl)aziridine (S-7).** To an ice-cold solution of 2-((2-

nitrophenyl)sulfonamido)ethyl methanesulfonate **S-6** (10 g, 30.11 mmol) in EtOAc (20 mL) was

added solution of KOH (3.4 g, 60.23 mmol) in water (10 mL). The resulting reaction mass was

stirred at rt for 1 h. After the completion of the reaction, the reaction mass was diluted with

EtOAc (100 mL). The organics part was washed with H$_2$O (3 times), saturated solution of citric

acid and brine respectively. The organic fraction was dried over anhydrous Na$_2$SO$_4$, filtered and

concentrated under reduced pressure to get desired product **S-7** as yellowish liquid (7 g), which

was further used without purification. $^1$H-NMR (400 MHz, CDCl$_3$): δ 8.19-8.21 (m, 1H), 7.74-7.80

(m, 3H) and 2.61 (s, 4H). LCMS found 229.14 [M+H]$^+$.

**Synthesis of *N*-(2-(9*H*-carbazol-9-yl)ethyl)-2-nitrobenzenesulfonamide (S-8).** To an ice-cold solution of 9*H*-carbazole (5.0 g, 29.9 mmol) in acetonitrile (60 mL) was added sodium hydride (60% in mineral oil, 1.5 g, 37.37 mmol) portion-wise. The reaction mixture stirred at 0°C for 15-20 min and followed by addition of a solution of 1-((2-nitrophenyl)sulfonyl)aziridine **S-7** (6.9 g, 29.9 mmol) in acetonitrile (40 mL). The resulting reaction mass was stirred at rt for 1 h. After the completion of the reaction, the reaction mass was diluted with water (20 mL), cooled to 0°C and adjust pH ~1 using concentrated HCl. The pale yellowish solid was filtered, washed with minimum quantity of methanol and diethyl ether. The solid was dried under vacuum to get desired product **S-8** as yellow solid (10 g, yield: 84%). $^1$H-NMR (400 MHz, DMSO-d$_6$): δ 8.26 (br s, 1H), 8.07 (d, *J*=7.2 Hz, 2H), 7.82 (d, *J*=7.6 Hz, 1H), 7.71 (t, *J*=7.2 Hz, 1H), 7.62 (d, *J*=7.2 Hz, 1H), 7.59 (d, *J*=7.6 Hz, 1H), 7.55 (d, *J*=8.0 Hz, 2H), 7.41 (t, *J*=6.8 Hz, 2H), 7.16 (t, *J*=6.8 Hz, 2H), 4.46-4.47 (m, 2H) and 3.38-3.40 (m, 2H). LCMS found 394.24 [M-H]$^+$.

**Synthesis of *N*-(2-(9*H*-carbazol-9-yl)ethyl)-*N*-ethyl-4-nitrobenzenesulfonamide (S-9).** To a solution of *N*-(2-(9*H*-carbazol-9-yl)ethyl)-2-nitrobenzenesulfonamide **S-8** (8.0 g, 20.25 mmol) in DMF (80 mL) was added K$_2$CO$_3$ (5.58 g, 40.50 mmol) and ethyl iodide (2.46 mL, 30.37 mmol). The resulting reaction mass stirred at rt for 16 h. After the completion of the reaction, the reaction mass was diluted with EtOAc (200 mL). The organic part was washed with ice-cold water (3 times) and brine respectively. The organic fraction was dried over anhydrous Na$_2$SO$_4$, filtered and concentrated under reduced pressure and crude was triturated with diethyl ether to get off-white solid product **S-9** (8.0 g, yield: 93%). $^1$H-NMR (400 MHz, DMSO-d$_6$): δ 8.23 (d, *J*=8.0 Hz, 2H), 7.90 (d, *J*=8.0 Hz, 1H), 7.80-7.85 (m, 2H), 7.69 (d, *J*=7.6 Hz, 1H), 7.58 (d, *J*=8.0 Hz, 2H), 7.44 (t, *J*=7.6 Hz, 2H), 7.19 (t, *J*=7.6 Hz, 2H), 4.59 (t, *J*=6.4 Hz, 2H), 3.65 (t, *J*=6.4 Hz, 2H), 3.29-3.32 (m, 2H) and 0.70 (t, *J*=7.6 Hz, 3H). LCMS found 424.29 [M+H]$^+$.

**Synthesis of *N*-(2-(3,6-diacetyl-9*H*-carbazol-9-yl)ethyl)-*N*-ethyl-4-nitrobenzenesulfonamide**

**(S-10).** To an ice-cold solution *N*-(2-(9*H*-carbazol-9-yl)ethyl)-*N*-ethyl-4-nitrobenzenesulfonamide

**S-9** (8.0 g, 18.91 mmol) in nitrobenzene (120 mL) was added aluminium chloride (12.6 g, 94.56

mmol) portion-wise and acetyl chloride (6.7 mL, 94.56 mmol). The resulting reaction mass was

stirred at 0°C for 1 h. After the completion of the reaction, the reaction mass was diluted with

water (100 mL) and extracted with EtOAc (3 x 100 mL). The combined organics were washed

with $H_2O$ (3 times) and brine respectively. The organic fraction was dried over anhydrous

$Na_2SO_4$, filtered and concentrated under reduced pressure. The crude was washed with *n*-

pentane (200 mL x 3 times) for removal of nitrobenzene and solid was filtered. The solid was

washed with diethyl ether to get desired product **S-10** as off-white solid (8.0 g, yield: 84%). $^1$H-

NMR (400 MHz, DMSO-d$_6$): $\delta$ 9.03 (s, 2H), 8.11 (d, *J*=8.8 Hz, 2H), 7.86-7.88 (m, 1H), 7.70-7.81

(m, 4H), 7.63-7.67 (m, 1H), 3.71-4.73 (m, 2H), 3.73-3.75 (m, 2H), 3.32-3.34 (m, 2H), 2.71 (s,

6H) and 0.77 (t, *J*=7.2 Hz, 3H). LCMS found 508.31 [M+H]$^+$.

**Synthesis of 1,1'-(9-(2-(ethylamino)ethyl)-9*H*-carbazole-3,6-diyl)bis(ethan-1-one) (S-11).** To

the solution of compound **S-10** (8.0 g, 15.77 mmol) in the mixture of $CHCl_3$:methanol (1:1, 300

mL) was added cesium carbonate (15.43 g, 47.33 mmol) and thiophenol (4.87 mL, 47.33 mmol).

The resulting reaction mixture was refluxed at 90°C for 2 h. After the completion of the reaction,

the reaction mass was concentrated under reduced pressure. The crude was diluted with water

(50 mL), cooled to 0°C and adjust pH ~1 using concentrated HCl. The aqueous part was

washed with ethyl acetate (3 times) for removal of organic impurities. The aqueous part was

basified till pH ~8 using saturated solution of sodium bicarbonate and extracted with the mixture

of DCM:MeOH (4:1, 3 times). The organic layer dried over anhydrous $Na_2SO_4$, filtered and

concentrated. The solid residue was washed with acetonitrile and diethyl ether respectively get

desired product **S-11** as off-white solid (4 g, yield: 80%). $^1$H-NMR (400 MHz, DMSO-d$_6$): $\delta$ 9.04

(s, 2H), 8.10 (d, $J$=8.4 Hz, 2H), 7.76 (d, $J$=8.4 Hz, 2H), 4.50 (t, $J$= 6.4 Hz, 2H), 3.32-3.34 (m, 2H), 2.90-2.93 (m, 2H), 2.70 (s, 6H), 1.78 (br s, 1H) and 0.88 (t, $J$=7.2 Hz, 3H). LCMS found 323.30 [M+H]$^+$.

**Synthesis of tert-butyl (2-((2-(3,6-diacetyl-9*H*-carbazol-9-yl)ethyl)(ethyl)amino)ethyl)carbamate (S-12).** To a solution of compound **S-11** (4.0 g, 12.42 mmol) in EtOAc (100 mL) was added $K_2CO_3$ (3.42 g, 24.84 mmol) and tert-butyl (2-bromoethyl)carbamate (3.34 g, 14.90 mmol). The resulting reaction mass was refluxed at 85°C for 48 h. After the completion of the reaction, the reaction mass was diluted with EtOAc (200 mL). The organic part was washed with ice-cold water (3 times) and brine respectively. The organic fraction was dried over anhydrous $Na_2SO_4$, filtered and concentrated under reduced pressure and crude was purified using normal phase chromatography eluting with 50% EtOAc/ hexane to get desired product as viscous liquid **S-12** (2.57 g, yield: 45%). $^1$H-NMR (400 MHz, DMSO-d$_6$): δ 9.05 (s, 2H), 8.10 (d, $J$=8.8 Hz, 2H), 7.76 (d, $J$=8.8 Hz, 2H), 7.41 (br s, 1H), 4.50-4.53 (m, 2H), 4.26-4.30 (m, 2H), 3.42-3.46 (m, 2H), 2.78-2.81 (m, 2H), 2.70 (s, 6H), 2.41-2.46 (m, 2H), 1.33 (s, 9H) and 0.72 (t, $J$=6.8 Hz, 3H). LCMS found 466.41 [M+H]$^+$.

**Synthesis of 1,1'-(9-(2-((2-aminoethyl)(ethyl)amino)ethyl)-9*H*-carbazole-3,6-diyl)bis(ethan-1-one) (S-13).** An ice-cold solution of compound **S-12** (2.57 g, 5.52 mmol) in TFA:DCM (1:1, 20 mL) was stirred at rt for 3 h. After the completion of the reaction, the reaction mass was concentrated under reduced pressure to get desired product **S-13** (2.0 g, quantitative yield) as a semi solid. $^1$H-NMR (400 MHz, DMSO-d$_6$): δ 9.11 (s, 2H), 8.15 (d, $J$=8.4 Hz, 2H), 7.85 (d, $J$=8.8 Hz, 2H), 4.89 (s, 2H), 4.26-4.30 (m, 2H), 3.56-3.58 (m, 2H), 3.42-3.46 (m, 2H), 3.36-3.38 (m, 2H), 3.25 (br s, 2H), 2.72 (s, 6H) and 1.22 (t, $J$=6.8 Hz, 3H). LCMS found 366.33 [M+H]$^+$.

**Synthesis of alkyne derivative of CBL0137 (S-14)**. To an ice cold solution of 3-(prop-2-yn-1-yloxy)propanoic acid **3** (0.35 g, 2.74 mmol) in DMF (10.0 mL) was added DIPEA (1.13 mL, 6.85 mmol) and HATU (1.56 g, 4.11 mmol). The resulting mixture was stirred under nitrogen atmosphere at 0°C for 15 min followed by addition of compound **S-13** (1.0 g, 2.74 mmol, 1 equivalent). The reaction mixture was then stirred at room temperature for 16 h. After the completion of the reaction, the reaction was diluted with ice cold water (30 mL) followed by extraction with EtOAc (3 x 50 mL). The combined organics were washed with brine, dried over anhydrous $Na_2SO_4$, filtered and concentrated under reduced pressure to get the crude products which was using normal phase column chromatography and eluted with 2% MeOH/DCM to get off white solid product (0.65 g, yield: 50%). $^1$H-NMR (400 MHz, DMSO-$d_6$): $\delta$ 9.04 (d, *J*=1.2 Hz, 2H), 8.10 (d, *J*=8.4 Hz, 2H), 7.76 (d, *J*=8.8 Hz, 2H), 7.48 (t, *J*=5.6 Hz, 1H), 4.50 (t, *J*=6.4 Hz, 2H), 4.04-4.05 (m, 2H), 3.55-3.58 (m, 2H), 2.80-2.89 (m, 4H), 2.70 (s, 6H), 2.50-2.54 (m, 1H), 2.42-2.47 (m, 4H), 2.18-2.21 (m, 2H) and 0.72 (t, *J*=7.2 Hz, 3H). LCMS found 476.51 [M+H]$^+$.

**Supplementary Figures**

**Table S1. Effect of trypanosome density on delayed cidal concentration.** Using either 1 x $10^5$ or 5 x $10^5$ trypanosomes/ml different amounts of stated compounds were used, as described in Legend to Figure 1, to obtain delayed cidal concentration (DCC).

**Table S2. RNAi primers used in this work.** Two RNAi constructs were synthesized for each protein studied. Each fragment was generated using primers whose sequences were determined with RNAit software (Redmond, 2003).

**Table S3. Primers used endogenous tagging.**

**Figure S1. ATP content of trypanosomes is not altered by CBL0137 treatment.** Trypanosomes (5 x $10^5$ cells/ml) were incubated for 1 h in HMI-9 medium in presence of DMSO (0.1%) or CBL0137 (180 nM or 290 nM or 800 nM). In control experiments, 2-deoxyglucose (2 mM) and sodium azide (3 mM) were added. Luminescence was converted to the amount of ATP per mg of protein (see *Materials and Methods*). Three biological replicates were studied. Horizontal lines represent means. A paired one-way ANOVA, using the DMSO condition as a control, was used to determine the possible statistical significance of differences in distribution of means between treatment and control groups.

**Figure S2. Six-hour CBL0137 treatment requires higher amount of drug to inhibit DNA synthesis.** *Panel A,* Scheme of the experimental protocol, and representative images for trypanosomes treated as described in the *Methods* section. For each condition, differential interference contrast microscopy (DIC), DAPI channel (blue), EdU channel (green), and a merge of DAPI and EdU images are presented. Images were captured using a DeltaVision II Olympus inverted microscope, and data were processed using Fiji (ImageJ, v 2.0.0). Data for integrated

intensity was processed using CellProfiler 3.1.9 (Soliman, 2015). **Panel B**, Analysis of the rescaled integrated EdU fluorescence intensity in nuclei. Bars indicate median and interquartile range. Kolmogorov-Smirnov test was used to assess statistical significance of differences in fluorescence intensities between DMSO and CBL0137 treatment groups $DCC_{50}$ (ns), and $DCC_{90}$ ($p = 7.5 \times 10^{-4}$).

**Figure S3. RPA1 knockdown in _T. brucei_.** Trypanosomes stably expressing V5-tagged RPA1 were transfected with an RNAi construct targeting RPA1. Parasites were induced with tetracycline (1 μg/ml) for 18 h. **Panel A**, Western-blot using $3 \times 10^6$ cell equivalents/lane of control (SM cells) or RPA1-RNAi line. Detection of V5 epitope on RPA1, and total protein followed protocols described in the legend to Figure 4. **Panel B**, Quantitation of changes in V5-RPA1 between induced and uninduced cells from four biological replicates. A paired Student t-test was used to determine the possible statistical significance of differences in mean values (_p_-value = 0.029). **Panel C,** Proliferation versus time curves for RPA1 knockdown and control trypanosomes. Data is from four biological replicates each with a starting density of $1 \times 10^5$ trypanosomes/ml. Cells that reached a density of $1 \times 10^6$ cells/ml were diluted 10-fold to continue the experiment. Cells density was determined with a Coulter-Counter. Two separate RNAi lines studied produced very similar results.   Horizontal lines represent means.

**Figure S4. Phenotypes associated with RPA2 knockdown.** SM **(**Single Marker) cells transfected with an RNAi construct against RPA2 were cultured in the HMI-9 medium containing tetracycline-free fetal bovine serum. Trypanosomes were harvested and inoculated into a fresh medium at a density of $1 \times 10^5$ cell/ml with and without tetracycline (1 μg/ml), followed by culturing for 24 h. Cells were fixed in paraformaldehyde (4%) and mounted with Vectashield containing

DAPI (5 µM). Trypanosomes were visualized using EVOS-FL microscope (Thermo Fisher), and

numbers of kinetoplasts and nuclei (per cell) were recorded. Anucleate (1K0N) trypanosomes are

highlighted with the black arrow.

**Figure S5. RPA1 knockdown does not inhibit the translation of proteins.**

***Panel A*** Western blot of newly synthesized protein. Trypanosomes bearing an RNAi construct

targeting RPA1 were induced with tetracycline (1 µg/ml) for 24 h. Tetracycline-induced (or

control) trypanosomes were rinsed in PBS-G and resuspended in RPMI medium without

methionine. Protocols for labeling and detection HPG incorporation into proteins are presented

in the legend for Figure 9. ***Panel B,*** Quantitation of the streptavidin fluorescence tracking

biotinylated HPG in protein. Possible statistical significance of differences in mean quantities of

HPG incorporation was determined with a paired Student t-test ($p = 0.9088$), using Prism 9.0

(Graphpad).

**Figure S6. Effect of CBL0137 treatment on total protein in trypanosomes. *Panel A,*** Total

protein at 0 h for different cell lines. ***Panel B***, Total protein in trypanosomes at time 0 h, and

after 6 h incubation with CBL0137 (730 nM). Clonal lines of *T. brucei* stably transfected with

epitope-tagged forms of V5-NRP1, V5-RPA1, and Tb427.03.1010-V5 were resuspended at 1 x

$10^5$ cells/ml and incubated with or without DMSO, or CBL0137 (725 nM) for 6 h. Cells were

counted, collected by centrifugation, and washed with PBS-G. Then, cells were lysed by

resuspension in SDS-sample buffer with 1 mM of β-mercaptoethanol to final density of 1 x $10^5$

of cells/µl for V5-NRP1 and Tb427.03.1010-V5, and 3 x $10^5$ cells/µl for V5-RPA1. Samples were

heated for 5 min at 95 ˚C. Each lane (for electrophoresis) was loaded with 10µl of sample.

Proteins were separated on TGX Fast-Cast™ Stain-free acrylamide (12%) gel (Bio-Rad,

Hercules, CA). The gel was exposed in ChemiDoc XRS+ (Bio-Rad) to obtain the image, after

which fluorescence was measured, quantitating signal for the entire lane using Fiji (ImageJ, v

MOLPHARM-AR-2021-000430R2

2.0.0). The experiment was performed three times for each cell line. A representative image for

the gel is found in Figure 7C (lower panel). A paired two-side Student t-test was used to

compare fluorescence data for untreated and CBL0137 treated conditions in all cell lines, using

Prism 9.0 (Graphpad). No statistically significant differences were found in fluorescence values.

*Panel C*, analysis of signal intensity of CK1.2 with different epitope tags in the c-terminus of the

protein; V5, or HA or Myc. Experimental procedures are like those described in Figure 7.

Trypanosomes (1 x 10$^6$ /lane) were used. A paired two-sided student t-test (in Prism 9.0

(Graphpad)) was used to evaluate possible statistically significant differences in means of

normalized steady-state amounts of tagged TbCK1.2 between control and CBL0137-treated

conditions. Horizontal lines represent means of the three biological replicates for each cell line.

LITERATURE CITED

Alibu VP, Storm L, Haile S, Clayton C and Horn D (2005) A doubly inducible system for RNA interference and rapid RNAi plasmid construction in Trypanosoma brucei. *Mol Biochem Parasitol* **139**(1): 75-82.

Guyett PJ, Xia S, Swinney DC, Pollastri MP and Mensa-Wilmot K (2016) Glycogen Synthase Kinase 3beta Promotes the Endocytosis of Transferrin in the African Trypanosome. *ACS Infect Dis* **2**(7): 518-528.

Redmond SV, Jamuna; Field, Mark C. (2003) Dynamics of Human Replication Protein A Subunit Distribution and Partitioning in the Cell Cycle. *Molecular & Biochemical Parasitology* **128**: 115-118.

Subramanya S and Mensa-Wilmot K (2006) Regulated cleavage of intracellular glycosylphosphatidylinositol in a trypanosome. Peroxisome-to-endoplasmic reticulum translocation of a phospholipase C. *FEBS J* **273**(10): 2110-2126.

Wirtz E, Leal S, Ochatt C and Cross GAM (1999) A tightly regulated inducible expression system for conditional gene knock-outs and dominant-negative genetics in Trypanosoma brucei. *Molecular and Biochemical Parasitology* **99**(89-101).
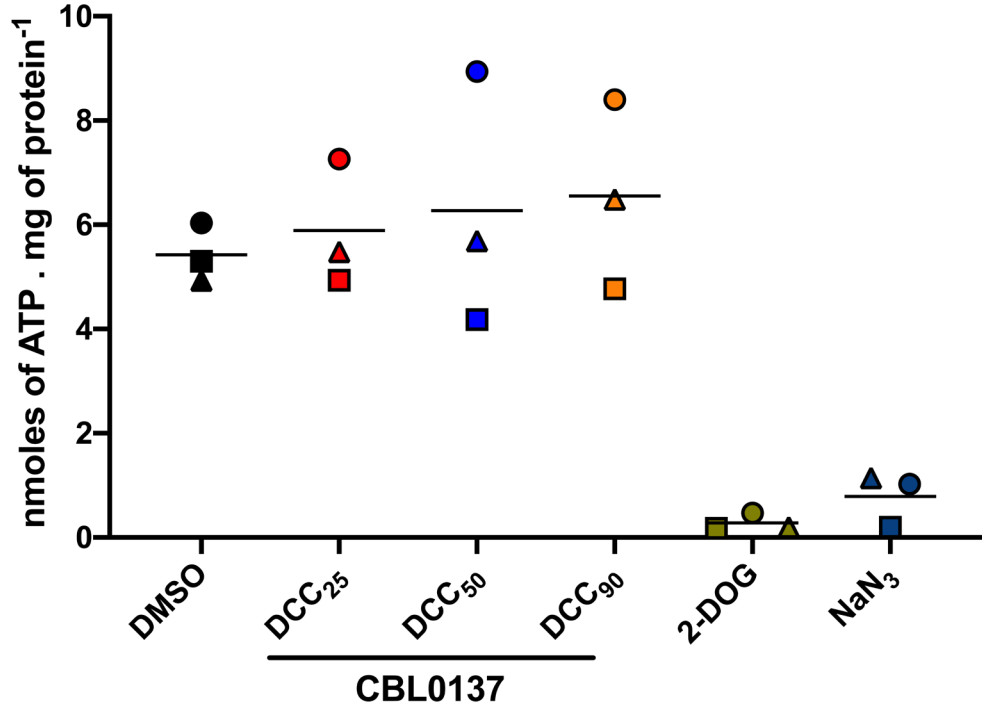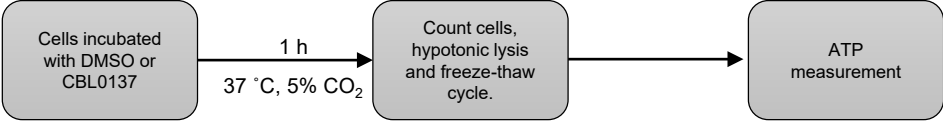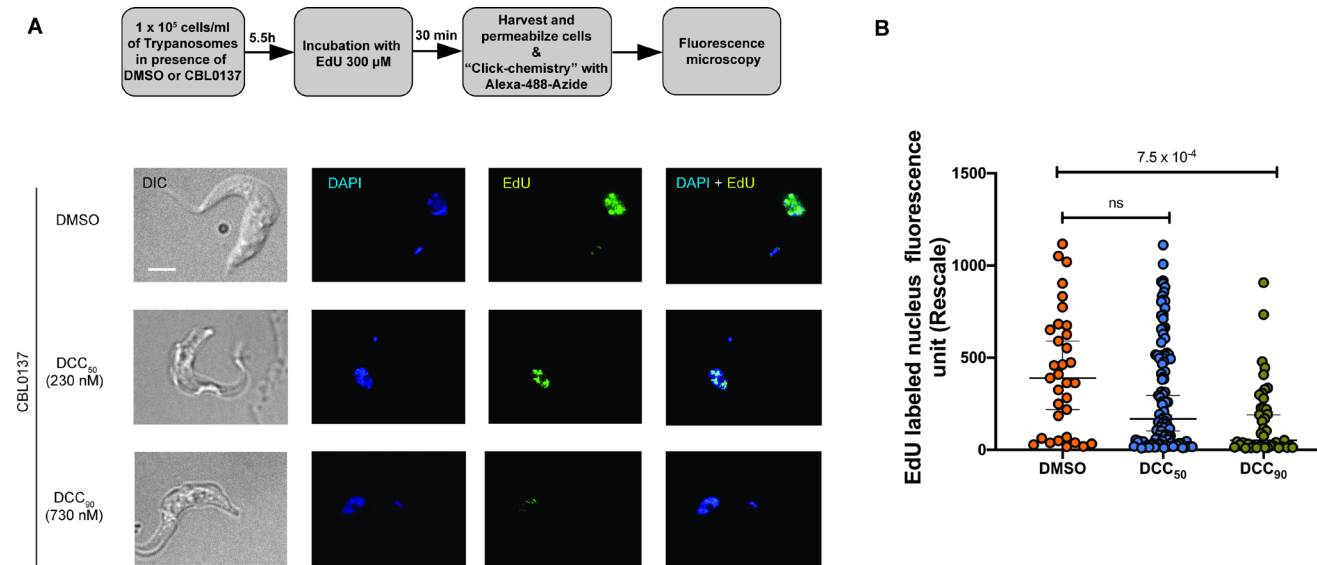
**Figure S1.**
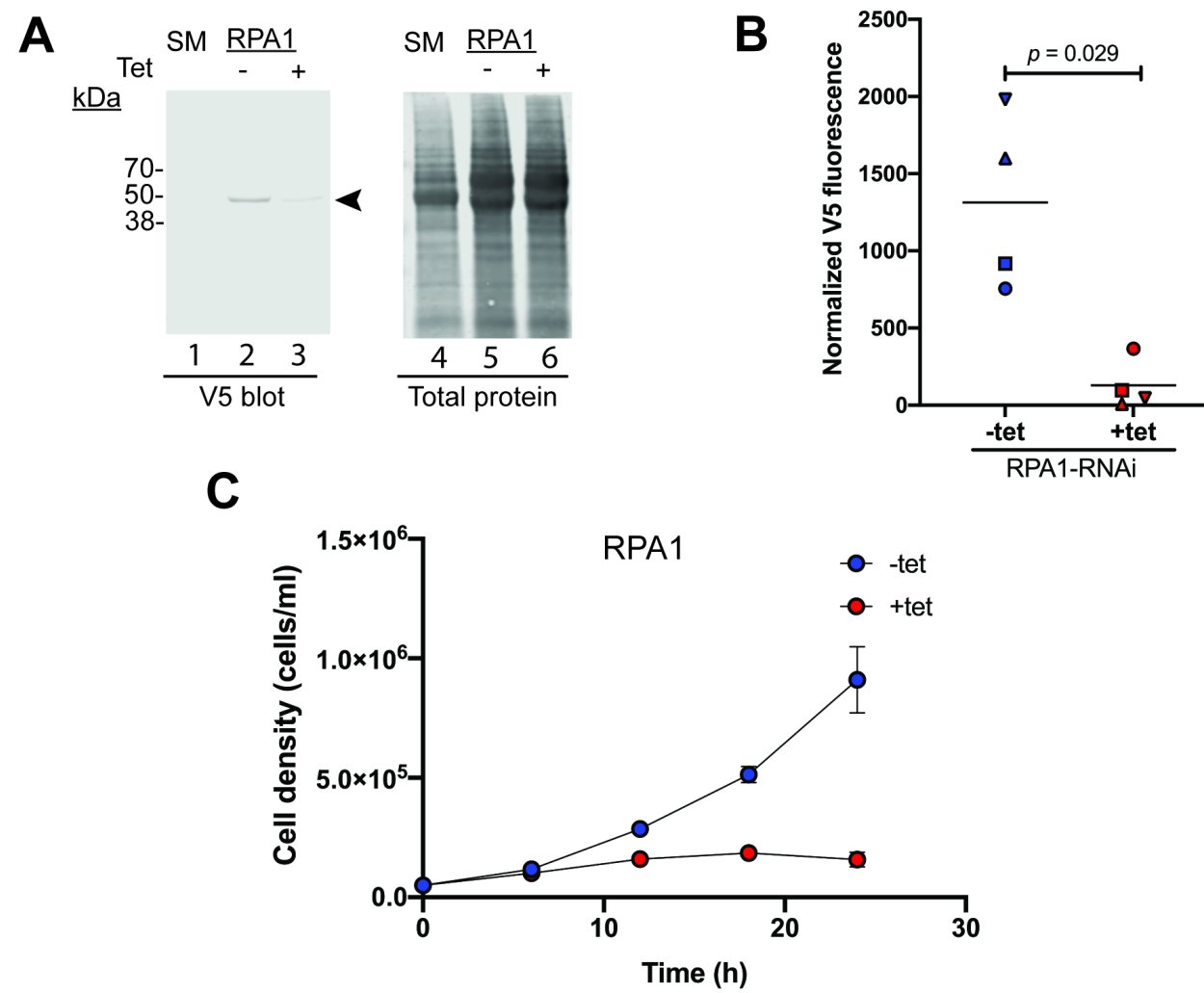
# Figure S2.

**Figure S3.**

**Figure S4.**
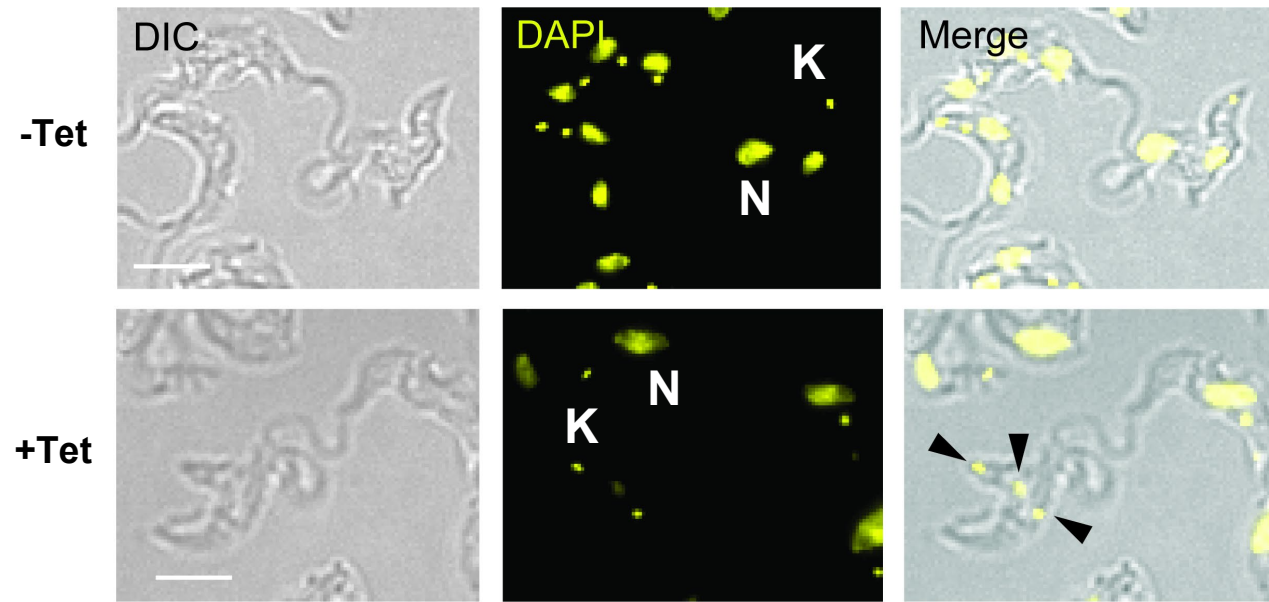


Arrows indicate enucleated cells

**Figure S5.**



A

SM    RPA1
tet  −  +   −  +

Total protein          Streptavidin

B

p = 0.7123    p = 0.9088

Streptavidin fluorescence (Normalized)

4×10⁵
3×10⁵
2×10⁵
1×10⁵
0

SM          RPA1

● −tet
● +tet

# Figure S6.



**A** Total protein

Stain-free fluorescence (Arbitrary unit)

$10^7$

$10^6$

$10^5$

| Cell line | | | |
|---|---|---|---|
| V5RPA1 | + | - | - |
| V5NRP1 | - | + | - |
| Tb.427.03.1010V5 | - | - | + |

**B** Effect of CBL0137 on total protein

ns    ns    ns

Stain-free fluorescence (arbitrary unit)

$10^7$

$10^6$

$10^5$

| CBL0137 | + | - | + | - | + | - |
|---|---|---|---|---|---|---|

V5-RPA1    V5-NRP1    1010-V5

**C**

CK1.2-**V5**

Normalized V5 fluorescence

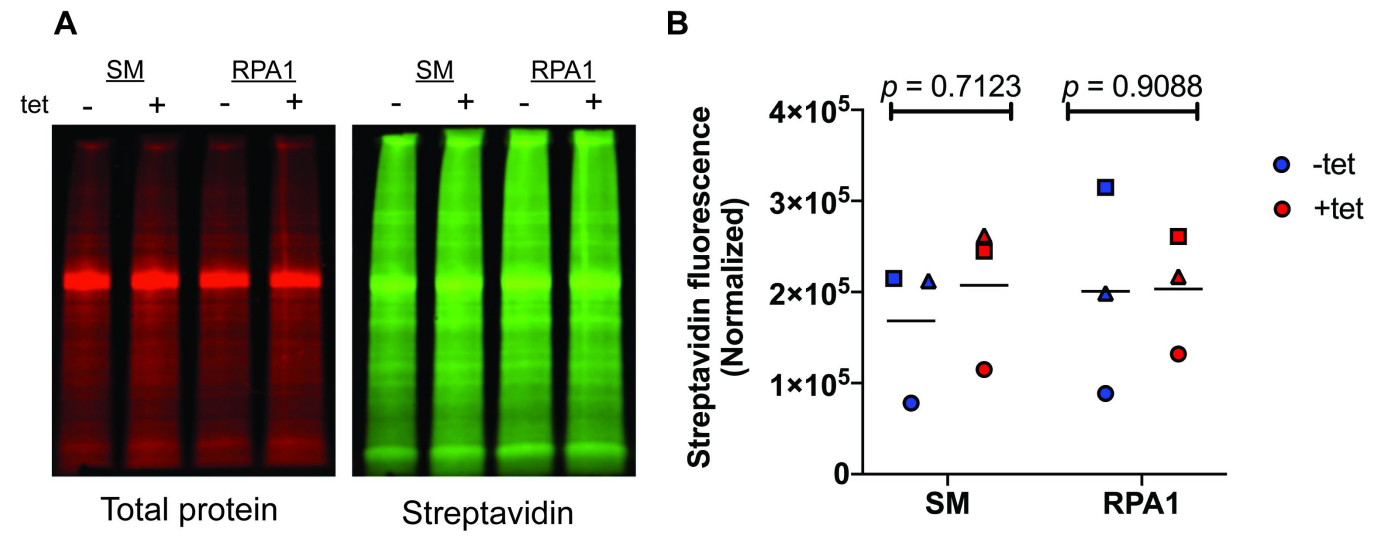$p$ = 0.01

1.2, 1.0, 0.8, 0.6

T= 0    DMSO 6h    CBL0137 6h

CK1.2-**HA**

Normalized HA fluorescence

$p$ = 2.5 x $10^{-4}$

1.2, 1.0, 0.8, 0.6

T= 0    DMSO 6h    CBL0137 6h

CK1.2-**Myc**

Normalized Myc fluorescence

$p$ = 1.2x $10^{-2}$

1.2, 1.0, 0.8, 0.6

T= 0    DMSO 6h    CBL0137 6h

**TableS1**

| Compound | Cell density (Cells/ml) | DCC$_{25}$ (µM) | DCC$_{50}$ (µM) | DCC$_{90}$ (µM) |
|---|---|---|---|---|
| CBL0137 | $1 \times 10^5$ | 0.12 | 0.23 | 0.73 |
| | $5 \times 10^5$ | 0.18 | 0.29 | 0.8 |
| Cycloheximide | $1 \times 10^5$ | 0.55 | 3.45 | 70 |
| | $5 \times 10^5$ | 2.84 | 9.03 | 86.74 |

**TableS2**

| RNAi construct | Forward 5`- 3` | Reverse 5`-3` |
|---|---|---|
| UMSBP2 -1 | tccgctcgaggaaataactgccaccggtgc | cgcggatccccatatttccgccacgcatg |
| UMSBP2-2 | tccgctcgagtttgcgagggaatgtccgaa | cgcggatccactcacgggcaatatgaccc |
| RPA2-1 | tccgctcgagtggtcgtgaggtgacacaag | cgcggatcctccatcagcgtacgtatggc |
| RPA2-2 | tccgctcgagcgagtgcagtcggtgttcaga | cgcggatcctctgaacaccgactgcactc |
| RPA1-1 | tagtacggatccaaccaatcgattccttgtcg | gtactactcgagccacattcaacacaacagcc |
| RPA1-2 | tccgctcgagctcgtcgattcccctacagc | cgcggatccttgtggacaggcatcgtacc |

**TableS3**

| Epitope tag | Orientation | Sequence |
|---|---|---|
| V5-UMSBP2 | Forward | aactagctttcctcaagtttttaaaacactttcagccaactttgcaagaacaatggccaagcctttgtctcaagaag |
| | Reverse | ttccctcgcaaagtggccgggctgaccgcaccggtggcagttatttccgccctcagcgcggtgccttttagcagtggaagcttcgtccgccatcgtagaatcgagaccgaggagagggttag |
| RPA2-myc | Forward | gctgctgctggcggtgctgctgctggtggtggacgcgcctgctacaactgtggccaacccggtcacctcagccgtgcctgccctgtgaaaggtaccgggcccccccctcgag |
| | Reverse | cgctttatggcgaaagtataggtaggcgtcgcgtgttcacattgcgaggacggacggtacatcggcacccctcctttactatcagttacctggcggccgctctagaactagtggat |
| V5-RPA1 | Forward | tatagactctagcgcacaagtaagcagaaaaatagtttacacatcaaatcgaaggaagtcggaaagttacttttattcatcacttcatggccaagcctttgtctcaagaag |
| | Reverse | cagacttgtccgtcacgcgagcgcgaatccaccacttgccgccaaggaatggcgacaaggaatcgattggttgaatctgttgttgtgatggctgctgcatcgtagaatcgagaccgaggagagggttag |